Cell Reports
Medicine

Article

Tolerance to colibactin correlates with homologous recombination proficiency and resistance to irinotecan in colorectal cancer cells

Graphical abstract

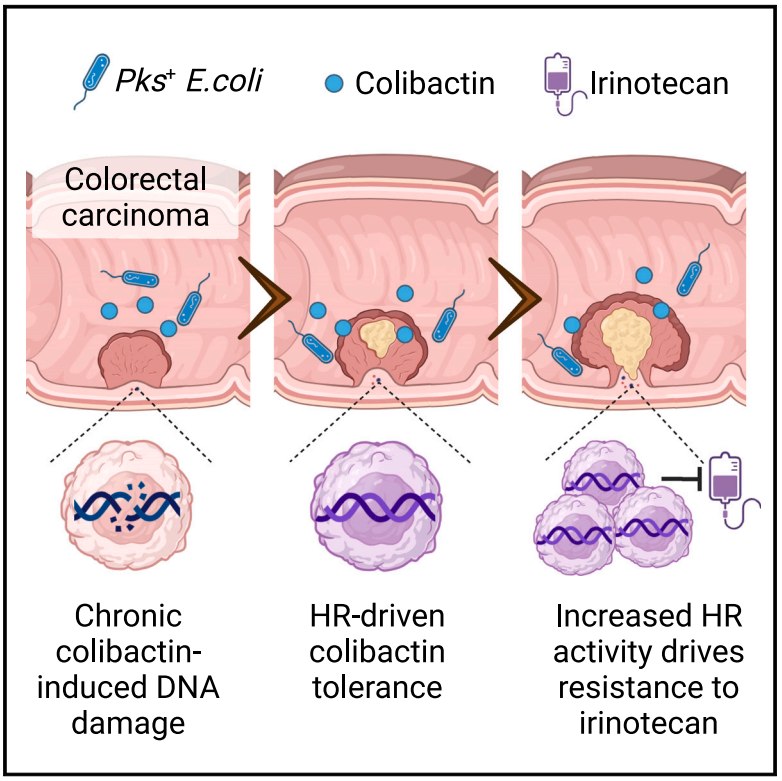

Authors

Alberto Sogari, Emanuele Rovera, Gaia Grasso, ..., Federica Di Nicolantonio, David Lembo, Alberto Bardelli

Correspondence

alberto.bardelli@unito.it

In brief

Sogari et al. show that cell response to the anti-colorectal cancer drug irinotecan and to the bacterial genotoxin colibactin, enriched in colorectal cancer, are correlated and are affected by homologous recombination (HR) proficiency. Chronic exposure to colibactin selects for cancer cells with restored HR activity and acquired resistance to irinotecan.

Highlights

- Homologous recombination (HR) discriminates cancer cells response to colibactin
- Sensitivity to colibactin correlates with response to SN38 in cell lines and PDOs
- Chronic exposure to colibactin selects HR-proficient, irinotecan-resistant cancer cells
- *Pks*$^{+}$ colorectal cancer patients show a trend toward poorer response to irinotecan

Sogari et al., 2024, Cell Reports Medicine *5*, 101376
February 20, 2024
https://doi.org/10.1016/j.xcrm.2023.101376

CellPress

Cell Reports Medicine

CellPress
OPEN ACCESS

Article

Tolerance to colibactin correlates with homologous recombination proficiency and resistance to irinotecan in colorectal cancer cells

Alberto Sogari,[1,2] Emanuele Rovera,[1,10] Gaia Grasso,[1,2] Elisa Mariella,[1,2] Nicole Megan Reilly,[3] Simona Lamba,[1] Gianluca Mauri,[2,4,5] Erika Durinikova,[3] Pietro Paolo Vitiello,[1,2] Annalisa Lorenzato,[1] Marco Avolio,[3] Eleonora Piumatti,[1,2] Emanuela Bonoldi,[6] Maria Costanza Aquilano,[6] Sabrina Arena,[3,7] Andrea Sartore-Bianchi,[4,5,8] Salvatore Siena,[4,5] Livio Trusolino,[3,7] Manuela Donalisio,[9] Mariangela Russo,[1,2] Federica Di Nicolantonio,[3,7] David Lembo,[9] and Alberto Bardelli[1,2,11,*]

[1]Department of Oncology, Molecular Biotechnology Center, University of Torino, Torino, Italy
[2]IFOM ETS – The AIRC Institute of Molecular Oncology, 20139 Milan, Italy
[3]Candiolo Cancer Institute, FPO–IRCCS, 10060 Candiolo, Italy
[4]Department of Oncology and Hemato-Oncology, Università degli Studi di Milano, Milan, Italy
[5]Department of Hematology, Oncology, and Molecular Medicine, Grande Ospedale Metropolitano Niguarda, Milan, Italy
[6]Department of Pathology, Grande Ospedale Metropolitano Niguarda, Milan, Italy
[7]Department of Oncology, University of Torino, 10060 Candiolo, Italy
[8]Division of Clinical Research and Innovation, Grande Ospedale Metropolitano Niguarda, Milan, Italy
[9]Department of Clinical and Biological Sciences, University of Torino, 10043 Orbassano, Italy
[10]Present address: Research Institute of Molecular Pathology (IMP), Vienna BioCenter (VBC), 1030 Vienna, Austria
[11]Lead contact
*Correspondence: alberto.bardelli@unito.it
https://doi.org/10.1016/j.xcrm.2023.101376

SUMMARY

The bacterial genotoxin colibactin promotes colorectal cancer (CRC) tumorigenesis, but systematic assessment of its impact on DNA repair is lacking, and its effect on response to DNA-damaging chemotherapeutics is unknown. We find that CRC cell lines display differential response to colibactin on the basis of homologous recombination (HR) proficiency. Sensitivity to colibactin is induced by inhibition of ATM, which regulates DNA double-strand break repair, and blunted by HR reconstitution. Conversely, CRC cells chronically infected with colibactin develop a tolerant phenotype characterized by restored HR activity. Notably, sensitivity to colibactin correlates with response to irinotecan active metabolite SN38, in both cell lines and patient-derived organoids. Moreover, CRC cells that acquire colibactin tolerance develop cross-resistance to SN38, and a trend toward poorer response to irinotecan is observed in a retrospective cohort of CRCs harboring colibactin genomic island. Our results shed insight into colibactin activity and provide translational evidence on its chemoresistance-promoting role in CRC.

INTRODUCTION

Gut microbiota represents an assortment of commensal microorganisms inhabiting the large intestine, mediating several functions of intestinal homeostasis.[1] Increasing evidence has shown that colorectal tumorigenesis is accompanied by significant transformation of the gut microbiota composition, with a decrease in commensal bacterial species and an enrichment of opportunistic, detrimental bacterial populations.[2,3] Moreover, specific species were found enriched in colorectal cancer (CRC) subtypes on the basis of staging, tumor site, and gender.[4,5] Importantly, certain bacterial strains have been shown to mediate several tumor-promoting mechanisms, including direct stimulation of cancer cell proliferation, promotion of an inflammatory microenvironment and generation of a pro-metastatic niche.[6,7] In addition, gut microbiota was found to have a role in driving resistance to anti-cancer treatments. For example, intratumoral bacteria have been shown to induce catabolism of gemcitabine and 5-fluorouracile,[8,9] and a recent study suggested a potential role of *Fusobacterium nucleatum* in driving resistance to platinum-based chemotherapies.[10]

In particular, a group of bacterial strains is claimed to be involved in colorectal tumorigenesis through the induction of mutations by several direct and indirect genotoxic mechanisms.[11] Among these, a significant fraction of Enterobacteriaceae, extraintestinal, and commensal *Escherichia coli* strains have been described to harbor the *pks* island, which encodes for several enzymes participating in the synthesis of the genotoxin colibactin.[12]

Numerous studies have described an enriched prevalence of the colibactin-encoding *pks* island in CRC patients compared with healthy controls, and a recent meta-analysis has found a

statistically significant higher risk for CRC development associated with gut colonization by colibactin-producing bacterial species.[13] Moreover, the Western diet was recently found to be associated with increased incidence of CRC characterized by higher *pks* island content in two large prospective cohorts.[14] Although the precise role of colibactin in colorectal tumorigenesis remains elusive, colibactin was proved to increase tumor formation in preclinical mouse models in association with other tumor-promoting factors[15,16] and was shown to be associated with tumors in distal colon and rectum.[17] Nevertheless, the overall genetic and molecular profile of *pks*-positive tumors remains obscure.[14]

From a molecular perspective, colibactin is able to alkylate DNA, forming inter-strand crosslinks and bulky DNA adducts and further inducing DNA double-strand breaks (DSBs).[12,18–20] Exposure to colibactin results in increased DNA damage, chromosomal aberrations, and mutation rate in infected cells.[21,22] Notably, *in vitro* exposure of normal colonic cells to colibactin promotes the acquisition of a Wnt-independent growth phenotype, characterized by increased proliferation rate coupled with high mutational load.[23] The result of colibactin activity is the formation of distinctive mutational signatures, which were found enriched in a subset of CRCs and associated with higher tumor mutational burden and increased copy number alterations.[17,24] Intriguingly, colibactin signatures are compatible with known mutational hotspots in cancer driver genes, including *APC*, which may suggest a role of colibactin in early CRC tumorigenesis.[17,23,24]

DSBs can be caused directly by colibactin through an oxidative, copper-dependent mechanism or may be the result of colibactin-induced replication stress (RS).[25,26] RS results from a variety of endogenous and exogenous genotoxic stressors that hamper or perturb DNA replication, leading to accumulation of single-strand breaks (SSBs) and DSBs.[27] Cells activate an intricate network of DNA damage response and repair (DDR) pathways to resolve damage and restore replication. This includes activation of the ATR-CHK1-WEE1 pathway, mainly in response to SSBs, with further activation of the base excision and mismatch repair pathways, and, for the repair of DSBs, activation of ATM, which further promotes homologous recombination (HR) and prevents toxic non-homologous end-joining (NHEJ).[27–29] Stalled replication forks are stabilized by RPA, while RAD51 acts as a master regulator for the recruitment of several DDR players (including Fanconi anemia and HR proteins).[30,31]

On the basis of the available evidence, while colibactin may exert a pro-tumorigenic role by driving the accumulation of mutations in normal colonic cells, failure in the activation of the DDR response results in cell cytotoxicity upon exposure to colibactin. Previous studies have shown that inhibition of specific DDR proteins (such as ATR for RS response and Ku80 for NHEJ) resulted in increased colibactin-induced cell cytotoxicity due to failed DNA damage repair.[18,22] This ultimately implies that colibactin acts as a "double-edged sword," which might promote tumor progression on one hand while creating an evolutionary bottleneck that selects proficiency in specific DNA repair pathways on the other. However, in this regard, available evidence is fragmentary and often relies on preclinical models not of colorectal origin, while a systematic effort in elucidating the DDR pathways needed to survive colibactin exposure has never been attempted.

We hypothesized that specific DNA repair pathways may influence tolerance to colibactin-induced DNA damage and cytotoxicity, and may be therefore positively selected by chronic exposure to this genotoxin. We also wanted to test the complementary hypothesis that colibactin drives CRC evolution and DNA repair machinery toward a phenotype that more proficiently repairs DNA damage induced by other exogenous sources, such as chemotherapeutic agents.

RESULTS

CRC cell lines show differential sensitivity to colibactin according to their ability to repair DNA damage

To study the cellular effects of exposure to colibactin, direct contact between colibactin-producing bacteria and eukaryotic cells is required.[21] We therefore exploited a coculture system taking advantage of a previously established model of *E. coli* DH10B with a BAC containing the colibactin-encoding *pks* island, together with the corresponding empty vector bacteria. We verified that this system was suitable to observe induction of DNA damage in cell lines infected with colibactin-producing *E. coli* (Figure 1A). To understand whether CRC cells with different genetic background could show differential sensitivity to colibactin genotoxic activity, we selected a representative panel of CRC cell lines, which were previously characterized in our laboratory,[32–34] and we screened them for sensitivity to colibactin. With this approach, we unveiled a subset of cell lines with exquisite sensitivity to colibactin, while another subgroup displayed marked tolerance (Figure 1B). In accordance with previous studies,[14] we found no clear association between sensitivity to colibactin and routinely assessed prognostic molecular biomarkers (Figure 1B). We then hypothesized that the ability to repair colibactin-induced DNA damage might better explain the colibactin-tolerant phenotype. We therefore monitored levels of DNA damage after exposure to colibactin in a representative subset of cells. In colibactin-tolerant cells, we observed a peak of DNA damage (marked by phosphorylation of H2AX at Serine 139[35]) at 24–48 h after infection, followed by attenuation in the following days, while colibactin-sensitive cells showed sustained levels of DNA damage up to 96 h after infection, suggesting that DNA damage was left unrepaired, resulting in increased cytotoxicity (Figure 1C).

Inactivation of ATM sensitizes cells to colibactin

To systematically and mechanistically characterize the pathways involved in colibactin-induced DNA damage repair, we exploited the CRISPR-Cas9 technology to generate a panel of isogenic cell lines, inactivating one key gene player for each DDR pathway (Figures S1A and S1B). We used the SW480 CRC cell line, which lacked genetic and functional defects in the DNA repair machinery and proved to be strongly colibactin tolerant.

We found that knockout (KO) of *ATM* (involved in DSBs repair and HR), *ATRIP* (RS), and *ERCC1* (NER) genes significantly sensitized cells to colibactin's genotoxicity (Figure 2A). In particular, cells with inactivation of *ATM* showed the most prominent

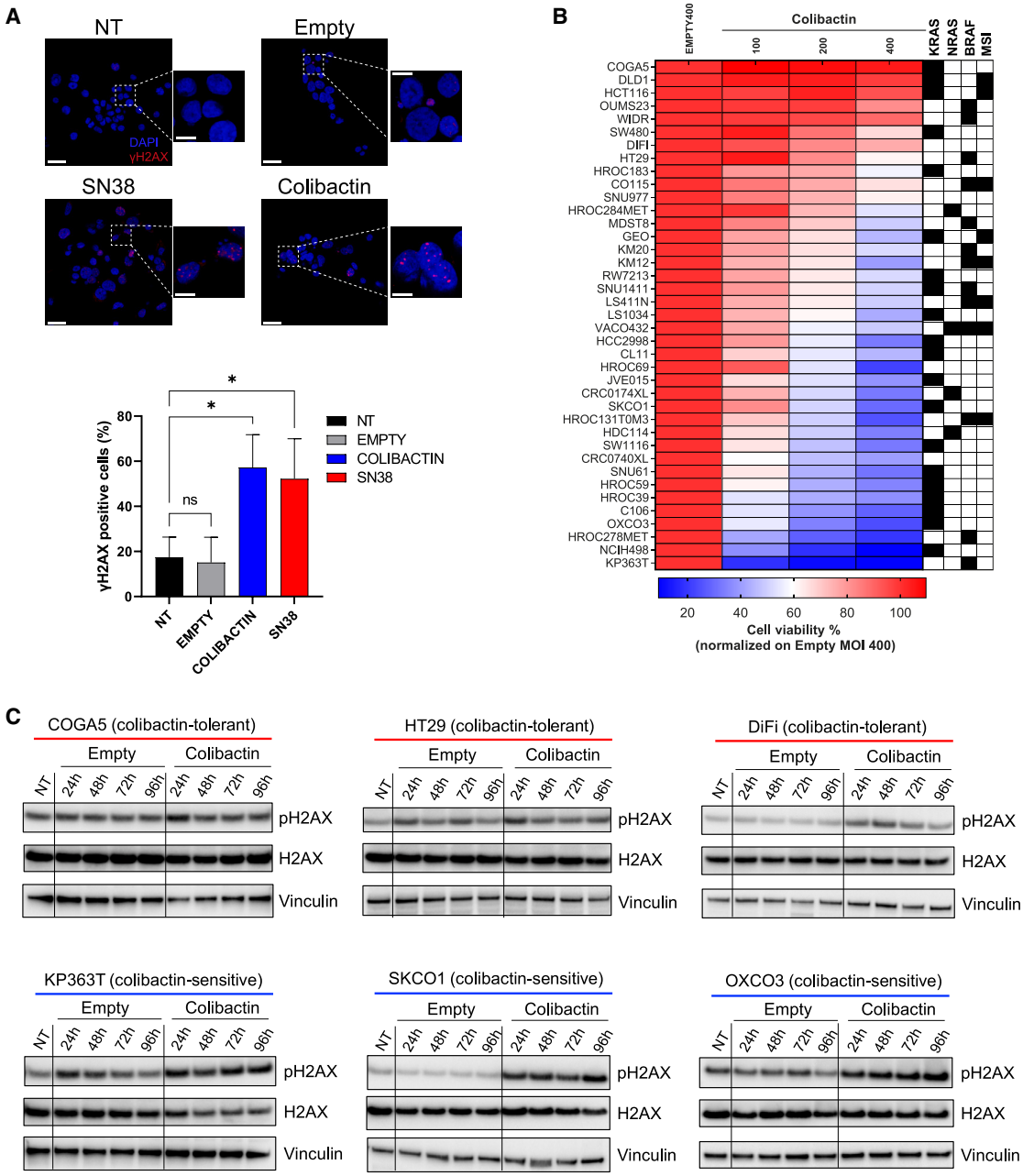

Figure 1. Proficient DNA damage repair discriminates colibactin-tolerant cells

(A) Top: representative images of DNA damage induced in KP363T cell line 48 h after infection with colibactin, compared with empty vector bacteria at a multiplicity of infection (MOI) of 200. NT, untreated (non-infected) cells. SN38 (2.5 nM) was used as positive control. Scale bar: 25 μm (10 μm in insets). Bottom: quantification of γH2AX foci. Results represent mean ± SD (n = 3, scoring at least 250 nuclei for each replicate). *p < 0.05 (one-way ANOVA with Bonferroni's multiple-comparisons test). Ns, not statistically significant.

(B) Left: heatmap showing mean residual cell viability 7 days after infection with colibactin at indicated MOIs, normalized on viability after infection with empty bacteria at an MOI of 400 (n = 2 for MDST8, JVE015, CRC0740XL, and OXCO3; n = 3 for the other cell lines). Right: *KRAS*, *NRAS*, and *BRAF* mutational status (black square marks mutation) and microsatellite instability phenotype (black square marks microsatellite unstable, MSI).

(C) Time course analysis of DNA damage levels (pH2AX) in colibactin-tolerant and sensitive cell lines after exposure to colibactin or empty bacteria. NT, untreated (non-infected) cells.

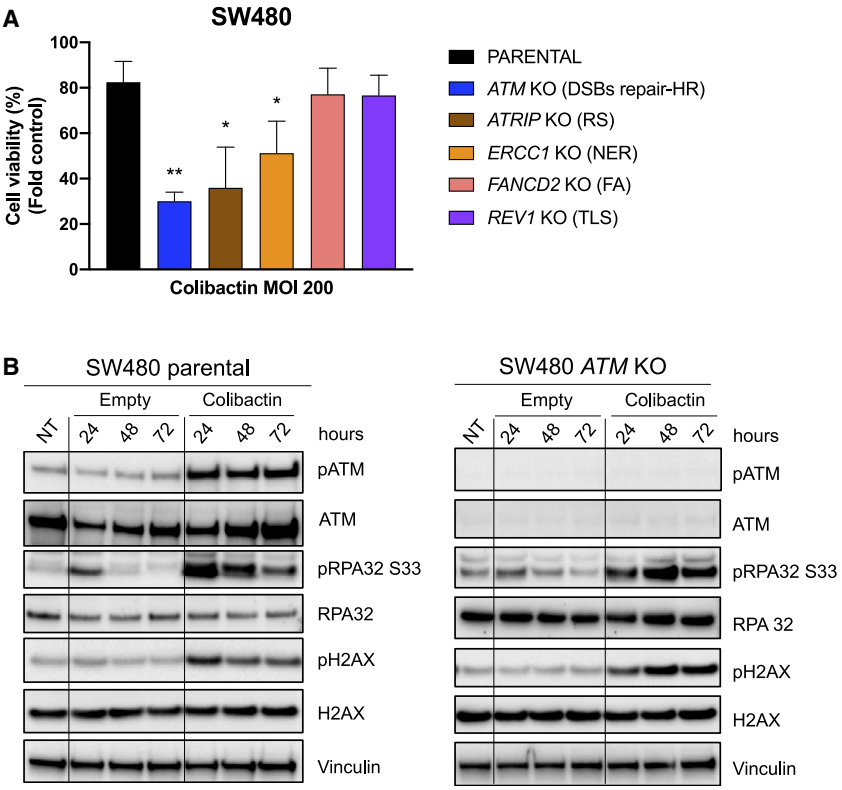

Figure 2. Genetic inactivation of *ATM* sensitizes cells to colibactin

(A) Cell viability of SW480 parental and isogenic DDR-KO cell lines 7 days after infection with colibactin, normalized on viability after infection with empty bacteria. Results represent mean ± SD (n = 3). *$p < 0.05$ and **$p < 0.01$ (compared with parental cells; one-way ANOVA with Bonferroni's multiple-comparisons test). DSBs, double-strand breaks; HR, homologous recombination; RS, replication stress; NER, nucleotide excision repair; FA, Fanconi anemia; TLS, translesion synthesis.

(B) Time course analysis of DNA damage (pH2AX) and replication stress (pRPA32) levels, together with activation of ATM (pATM), after exposure to colibactin or empty bacteria at indicated time points. NT, untreated (non-infected) cells.

See also Figure S1.

effect (Figures 2A and S1C). Moreover, treatment with ATM inhibitor AZD0156 was sufficient to sensitize SW480 parental and isogenic DDR-KO cells to colibactin (Figure S1D). It should be noted that *ATRIP*-KO cells showed marked sensitivity to the ATM inhibitor alone, even when using a lower drug concentration, in accordance with the known synthetic lethal effect between abrogation of the ATR and the ATM pathways.[36] Nevertheless, an additional effect on sensitization to colibactin was still measurable in this cell model.

The results obtained with *ATM* and *ATRIP* KO suggested that RS induced by colibactin resulted in increased DSBs, and that overall the intertwined processes of HR and RS response could be key for colibactin-induced DNA damage repair. Indeed, by monitoring the activation of DDR response in SW480 parental cells by Western Blot we found that colibactin induced DNA damage at 24 h, which was accompanied by increased levels of RS marker phospho-RPA32, but both attenuated over time (Figure 2B). On the contrary, the *ATM*-KO cells experienced sustained levels of (unresolved) DNA damage and RS (Figure 2B).

HR proficiency correlates with response to colibactin

Given the involvement of ATM in the HR pathway, we hypothesized that HR status could explain differential sensitivity to colibactin. Intriguingly, we previously showed that KP363T and HROC278MET, clustering among the most colibactin-sensitive cell lines (see Figure 1B), harbored loss of *RAD51C*, a RAD51 paralog involved in HR-mediated DNA damage repair, and proved to be HR deficient[33,37];while in contrast WiDr and DiFi cells, clustering among colibactin-tolerant cell lines, proved to be HR proficient.[34] In line with our hypothesis, we found that cell lines that failed to form RAD51 foci after exposure to ionizing radiations, which are known to induce DSBs,[34] tended to cluster among the most colibactin-sensitive cell lines (Figure S2). On the other hand, we reasoned that colibactin-tolerant cells should be HR proficient. We therefore measured RAD51 foci formation as a marker of HR activation after exposure to colibactin and found that colibactin-tolerant cell lines showed increased levels of RAD51 foci compared with sensitive ones (Figures 3A–3C). To further validate our hypothesis, we tested sensitivity to colibactin in a small panel of ovarian cancer cell lines, a cancer type where a significant subset of tumors shows HR deficiency[38] and in which previous work described the enrichment of colibactin mutational signature.[24] We therefore selected A2780, a *BRCA1/2* wild-type cell line that was previously characterized as HR proficient,[39] and UWB1.289 cell line, which harbors an inactivating mutation in *BRCA1*, thus being HR deficient.[40] We validated the HR profile of each cell line by testing their sensitivity to PARP inhibitor olaparib (Figure 3D). Notably, we found that the HR-deficient UWB1.289 cell line was significantly more sensitive to colibactin than the HR-proficient A2780 cells (Figure 3E).

Restoration of HR confers tolerance to colibactin

We next hypothesized that reconstituting HR proficiency could render HR-deficient, colibactin-sensitive cell lines tolerant to colibactin-induced cytotoxicity. To this end, we exploited two different approaches.

First, we took advantage of a previously reported, modified UWB1.289 derivative model with exogenous re-expression of *BRCA1*, which confers restoration of HR proficiency.[40] Accordingly, we found that the UWB1.289 + BRCA1 derivative cell line showed a significant increase in residual cell viability upon treatment with olaparib (Figure 4A) and concomitantly showed significantly increased tolerance to colibactin genotoxic activity (Figure 4B).

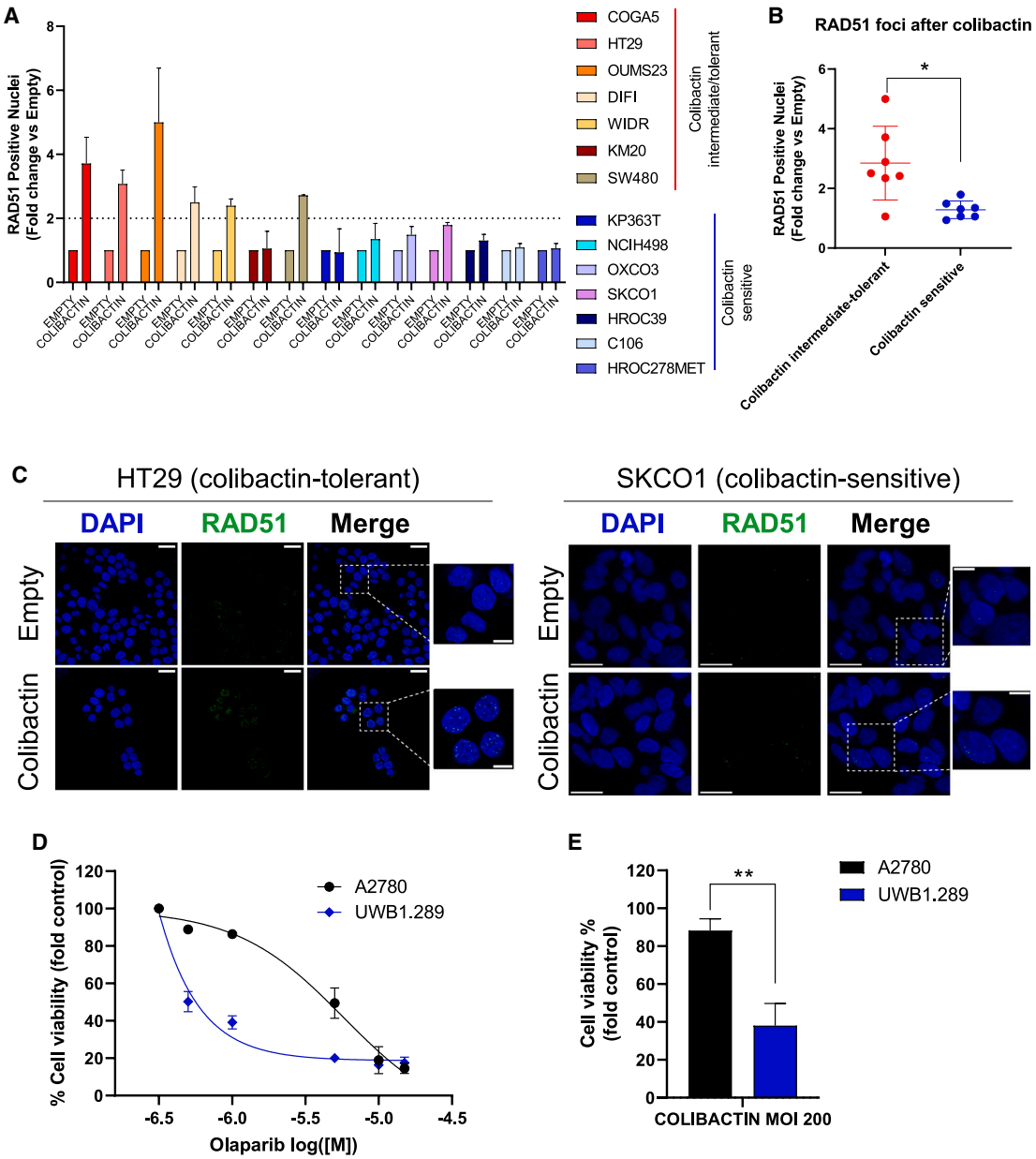

Figure 3. Colibactin-tolerant cell lines are characterized by proficient homologous recombination

(A) Quantification of nuclear RAD51 foci in colibactin-intermediate/tolerant and colibactin-sensitive cells 24 h after infection, normalized on exposure to empty bacteria. Results represent mean ± SD (n = 2, scoring at least 200 nuclei for each replicate).

(B) Statistical significance for RAD51 foci formation between colibactin-intermediate/tolerant and sensitive cells. Lines represent mean ± SD. *$p < 0.05$ (Mann-Whitney test).

(C) Representative images of RAD51 foci 24 h after infection with colibactin or empty bacteria at an MOI of 200. Scale bar: 25 μm (10 μm in insets).

(D) Sensitivity to olaparib of ovarian cancer cell lines after 7 days of treatment. Results represent mean ± SD (n = 3).

(E) Cell viability of ovarian cancer cell lines 7 days after infection with colibactin, normalized on viability after infection with empty bacteria. Results represent mean ± SD (n = 3). **$p < 0.01$ (Student's t test).

See also Figure S2.

In parallel, we generated olaparib-resistant CRC cells with acquired resistance to olaparib by constant exposure of HR-deficient KP363T and HROC278MET cells to olaparib until a resistant population emerged (Figure 4C). Previous evidence suggested that restoration of HR was a mechanism of acquired resistance to olaparib.[41] In fact, olaparib-resistant KP363T and HROC278MET derivatives showed proficient activation of HR on the basis of RAD51 foci formation upon exposure to colibactin

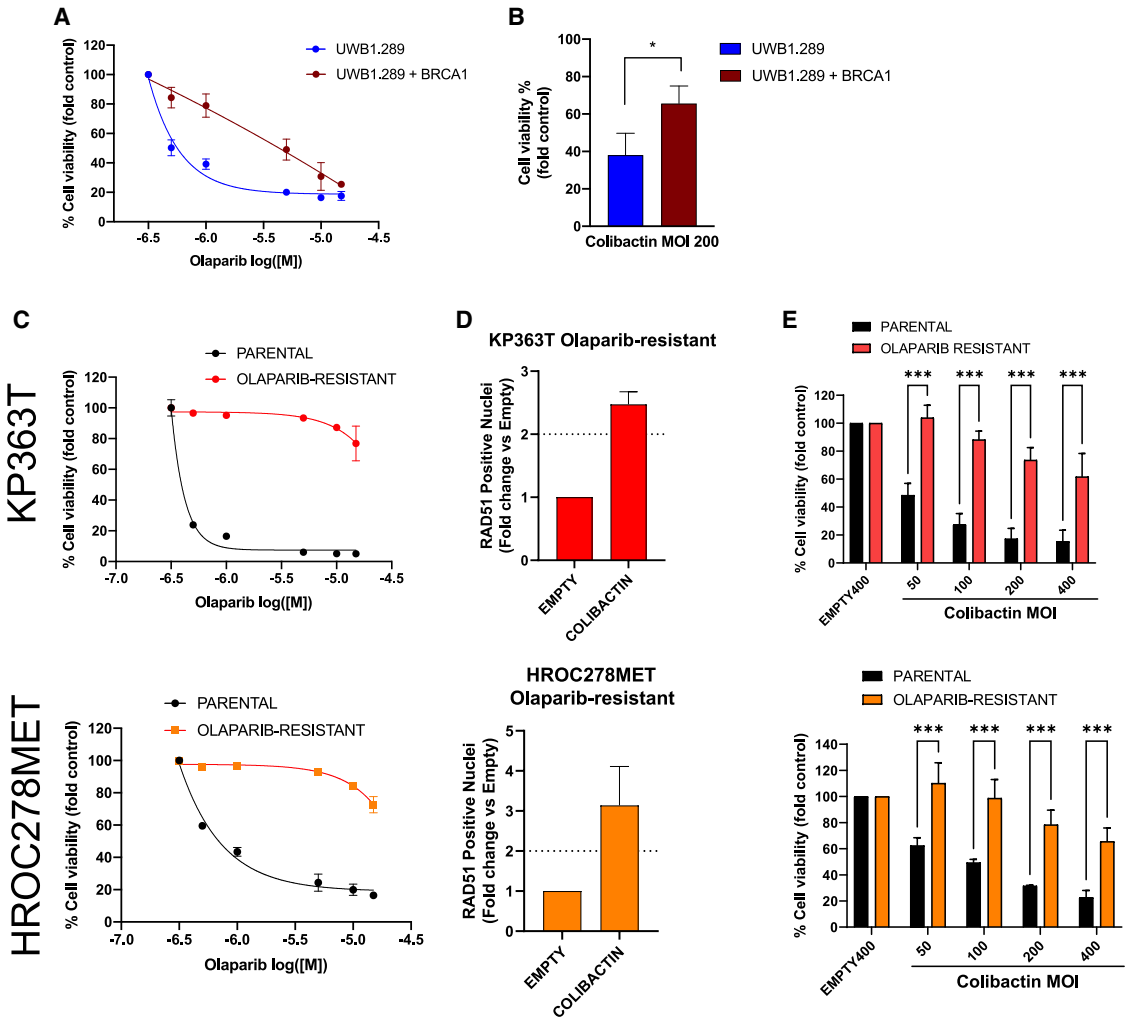

Figure 4. Impact of homologous recombination reconstitution in colibactin-sensitive cells

(A) Sensitivity to olaparib of UWB1.289 with restored *BRCA1* expression compared with their parental counterpart. Results represent mean ± SD (n = 3; data for UWB1.289 parental cells as in Figure 3E for comparison).

(B) Cell viability of UWB1.289 + BRCA1 and parental cells 7 days after infection with colibactin, normalized on viability after infection with empty bacteria. Results represent mean ± SD (n = 3). *p < 0.05 (Student's t test).

(C) Sensitivity to olaparib in KP363T (top) and HROC278MET (bottom) parental cell lines and corresponding olaparib-resistant derivatives. Results represent mean ± SD (n = 3).

(D) Quantification of nuclear RAD51 foci in indicated cell lines 24 h after infection, normalized on exposure to empty bacteria. Results represent mean ± SD (n = 2, scoring at least 200 nuclei for each replicate).

(E) Cell viability after infection with colibactin at indicated MOIs, normalized on viability after infection with empty bacteria at an MOI of 400, in KP363T (top) and HROC278MET (bottom) parental cell lines and olaparib-resistant derivatives. Results represent mean ± SD (n = 3). ***p < 0.001 (two-way ANOVA with Bonferroni's multiple-comparisons test).

See also Figure S3.

(Figure 4D; Figure S3A) and the functional pDRGFP/pCBASce-I assay[42] in olaparib-resistant KP363T (Figures S3B and S3C). Therefore, we hypothesized that this HR-proficient phenotype selected by olaparib could further drive resistance to colibactin. Indeed, we found that olaparib-resistant cells were significantly more tolerant to colibactin (Figure 4E). In particular, KP363T olaparib-resistant cells show 2.1- to 4.2-fold increase in cell viability when exposed to colibactin compared with the parental counterpart, and concomitantly display a comparable 5.8-fold increase when treated with olaparib at clinically relevant concentration (1 μM). Similarly, HROC278MET olaparib-resistant cells show 1.8- to 2.9-fold increase in cell viability after infection with colibactin and a 2.2-fold increase after treatment with olaparib 1 μM.

Chronic exposure to colibactin selects HR-proficient cells

Intrigued by these results, we next wondered whether chronic exposure to colibactin (similarly to what is presumed to occur

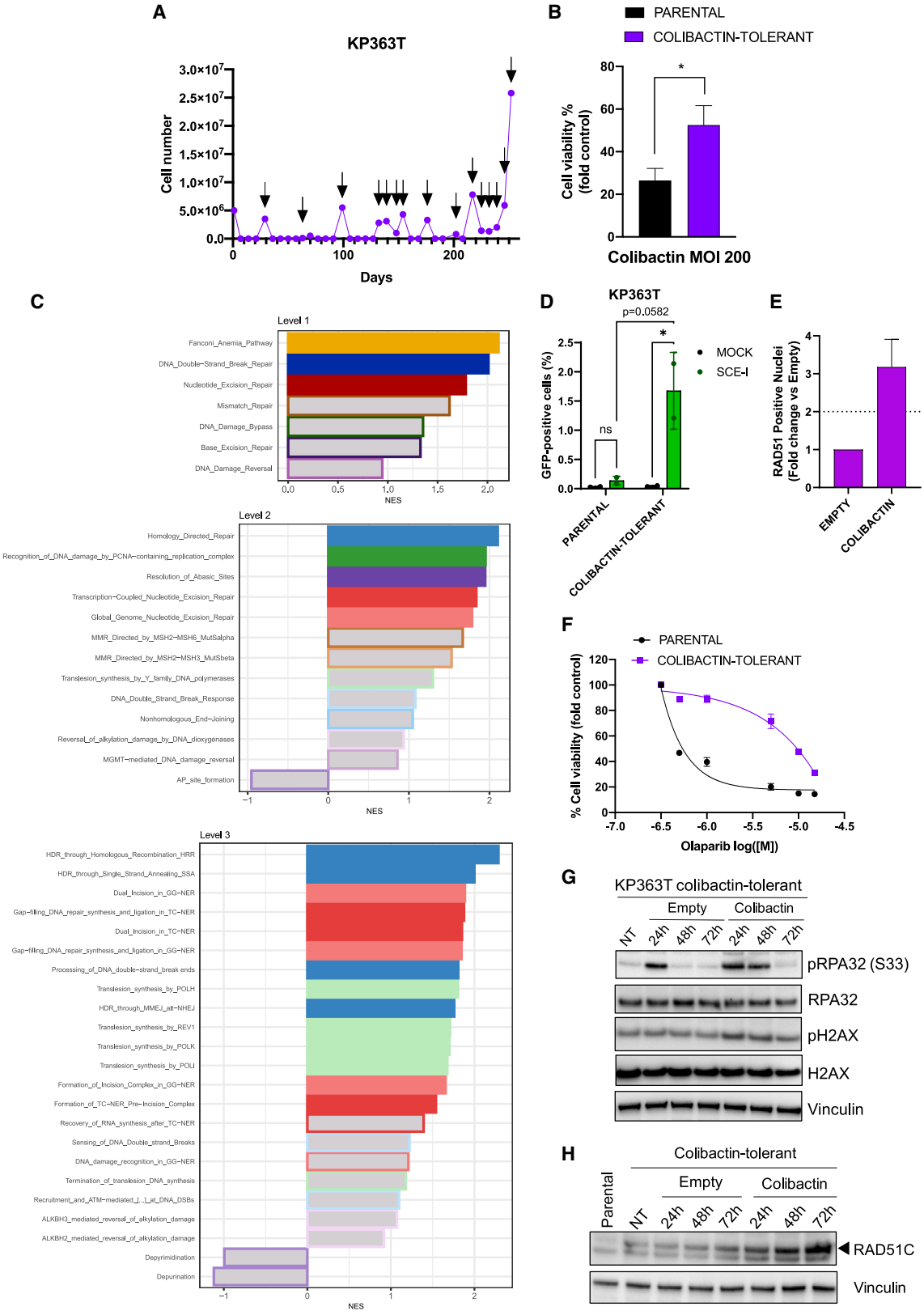

(legend on next page)

during tumorigenesis) could modulate HR status. To this end, we chronically exposed the HR-deficient, colibactin-sensitive KP363T cell line to serial infections with colibactin, until a colibactin-tolerant population eventually emerged (Figures 5A and 5B).

In order to understand the impact of prolonged exposure to colibactin on the DNA repair machinery of these cells, we performed RNA sequencing (RNA-seq). Specifically, we carried out a differential gene expression analysis to compare the transcriptomic profile of KP363T cells that acquired tolerance to colibactin with that of control parental cells exposed to empty vector bacteria for the same number of infections. We then performed pre-ranked gene set enrichment analysis (GSEA) exploiting the publicly available and peer-reviewed Reactome protein interactions database[43] to build multiple gene sets comprising DNA repair genes (Table S1). Following Reactome hierarchical organization of DNA repair, we decided to first classify genes into 7 DNA repair pathways (level 1), further stratified in different pathway branches (level 2) and branch activities (level 3), and performed GSEA on the three levels independently. With this approach, we found that several DNA repair pathways showed a statistically significant enrichment among the upregulated genes, suggesting that a general rewiring of the DNA repair machinery occurred after prolonged exposure to colibactin (Figure 5C). At level 1, the Fanconi anemia pathway scored as the most enriched gene set on the basis of the normalized enrichment score (NES). However, when we stratified the DNA DSB repair gene set (which comprises both homology- and non-homology-mediated repair pathways, such as HR and NHEJ, respectively) in levels 2 and 3, homology-directed repair through HR scored as the most enriched pathway (Figures 5C, S4A, and S4B).

As functional validation, quantification of HR proficiency with the pDRGFP/pCBASce-I assay unveiled a significant activation of the HR pathway in KP363T cells that developed tolerance colibactin (Figures 5D and S4C). Similarly, colibactin-tolerant KP363T showed increased RAD51 foci formation upon acute re-exposure to colibactin (Figures 5E and S4D; see Figure 3 for RAD51 foci measurement in in the parental counterpart for comparison). This was further confirmed by the acquisition of cross-resistance to PARP inhibition (Figure 5F).

Notably, these cells displayed a pattern of DDR markers closely similar to that we observed in colibactin-tolerant cells (see Figure 1C), with a peak of damage (phospho-H2AX) and RS (phospho-RPA) which tended to attenuate over time by ongoing DNA damage repair (Figure 5G). As previously mentioned, parental KP363T harbor loss of *RAD51C* expression as a driver of HR deficiency. Notably, RNA-seq analysis showed that colibactin-tolerant KP363T cells restored expression of *RAD51C* (Figure S4B). We therefore assessed protein expression of RAD51C in the colibactin-tolerant KP363T cells and we observed that not only did these cells re-express RAD51C after chronic exposure to colibactin, but its protein levels further increased over time after acute re-infection (Figure 5H).

Tolerance to colibactin correlates with resistance to irinotecan active metabolite SN38

Given the strong genotoxic activity exerted by colibactin, we hypothesized that shared DNA repair mechanisms could underlie sensitivity to both colibactin and chemotherapeutic drugs which are administered as standard of care in metastatic CRC (mCRC), namely 5-fluorouracil, oxaliplatin, and SN38 (the active metabolite of irinotecan).[44] To investigate our hypothesis, we took advantage of a systematic effort of pharmacological annotation of a CRC cell line collection previously established in our lab.[33] We crossed chemotherapy sensitivity with response to colibactin and found that cell lines most sensitive to colibactin also showed a profound sensitivity to SN38, and that colibactin-tolerant cells were also cross-resistant to SN38 (Figures 6A and 6B). Importantly, although some cell lines with sensitivity to colibactin were also significantly sensitive to oxaliplatin, correlation between colibactin and oxaliplatin sensitivity failed to reach statistical significance (Figure S5A).

To corroborate our findings, we found that KP363T with acquired tolerance to colibactin also showed increased resistance to clinically relevant concentrations of SN38 but not to oxaliplatin (Figure 6C). Notably, KP363T weekly re-infected with empty vector bacteria for the same number of infections did not acquire resistance to olaparib or to other chemotherapeutic agents (Figure S5B). Similar results were reproduced in the additional cell model HROC39, which after repeated rounds of

Figure 5. Exposure to colibactin selects HR-proficient cells

(A) KP363T cells were longitudinally re-infected with colibactin until a tolerant population capable of surviving to colibactin was selected. Arrows mark infections with colibactin.

(B) Cell viability of KP363T parental cells and colibactin-tolerant derivative 7 days after infection with colibactin, normalized on viability after infection with empty bacteria. Results represent mean ± SD (n = 3). *p < 0.05 (Student's t test).

(C) Gene set enrichment analysis of KP363T colibactin-tolerant cells. DNA repair gene sets derived from the Reactome Database are stratified in three levels (analyzed independently) and ranked by normalized enrichment score (NES). Gene sets with statistically significant enrichment (false discovery rate [FDR] < 0.5) are colored, while gray-filled bars indicate non-significantly enriched gene sets (FDR > 0.5). Colors of bar filling and borders refer to the hierarchical organization of the pathways based on Reactome annotation (i.e., gene sets with a given color at levels 2 and 3 branch from a parental pathway in level 1 colored with the same color nuance but darker).

(D) Quantification of HR activity compared with mock in KP363T parental and colibactin-tolerant cells. Results represent mean ± SD (n = 2). *p < 0.05 (two-way ANOVA with Bonferroni's multiple-tests correction). Ns, not statistically significant.

(E) Quantification of nuclear RAD51 foci in colibactin-tolerant KP363T cells 24 h after infection, normalized on exposure to empty bacteria. Results represent mean ± SD (n = 2, scoring at least 200 nuclei for each replicate).

(F) Sensitivity to olaparib in KP363T parental cell line and colibactin-tolerant derivative. Results represent mean ± SD (n = 3).

(G) Time course analysis of DNA damage and replication stress levels in KP363T colibactin-tolerant derivative. NT, untreated (non-infected) cells.

(H) Expression of RAD51C in KP363T colibactin-tolerant cells after infection with colibactin or empty bacteria, compared with basal levels in parental cells. NT, untreated (non-infected) cells.

See also Figure S4.

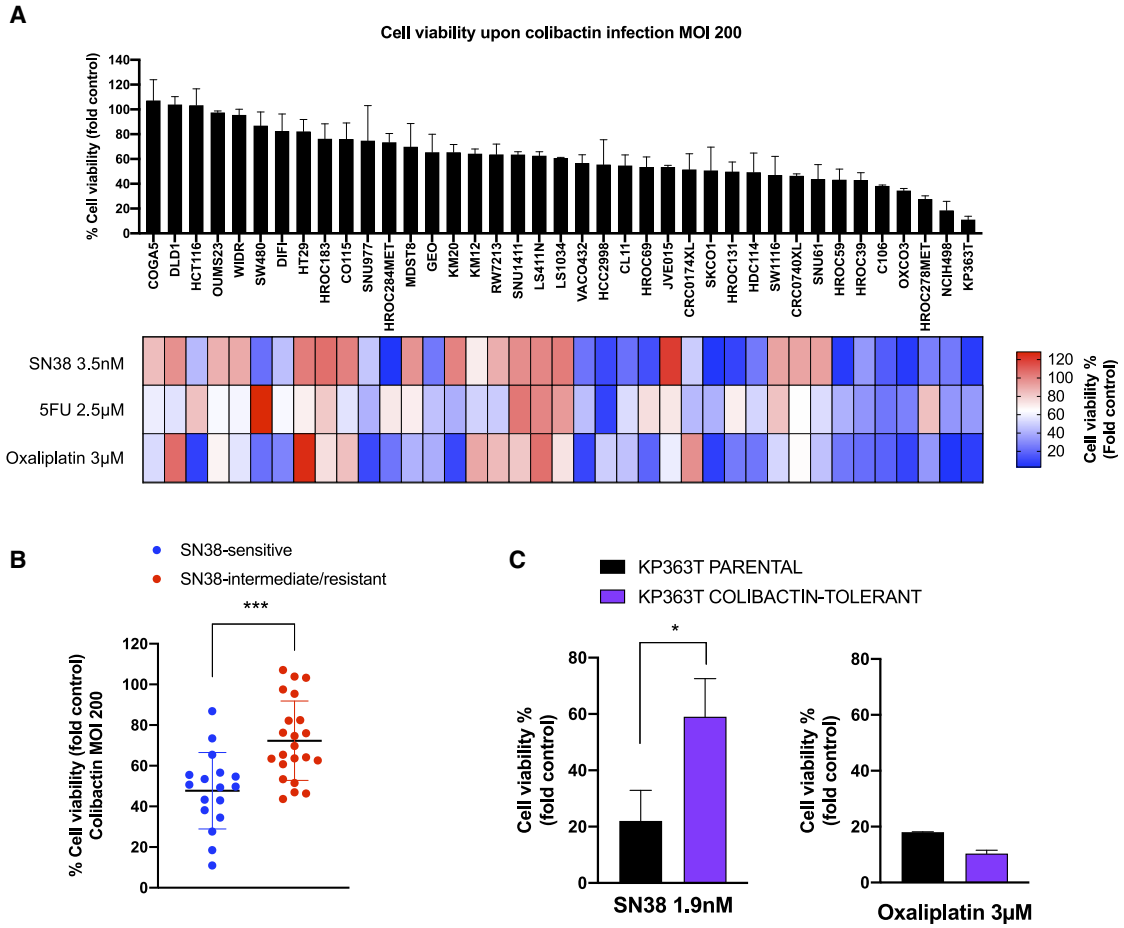

(legend on next page)

infection acquired a colibactin-tolerant, chemo-resistant phenotype (Figures S5C–S5F).

We reasoned that the correlation between the sensitivity profiles to colibactin and SN38 could be explained by similarities in the way these molecules impinge on the DNA repair machinery. Therefore, we analyzed activation of the DDR response after exposure to colibactin, SN38, or oxaliplatin. Although all the three agents induced various degree of RS (as assessed by phospho-RPA and phospho-CHK1), both colibactin and SN38 strongly activated phospho-ATM and its downstream effector phospho-CHK2 in a similar fashion and more significantly compared with treatment with oxaliplatin (Figure 6D). This suggests that DNA DSBs induced by both colibactin and SN38 are sensed by ATM, but downstream activity of the HR pathway controls response to both colibactin and SN38. In fact, colibactin-tolerant COGA5 and HT29 cells showed formation of RAD51 foci in response to colibactin, in contrast to colibactin-sensitive KP363T and HROC39 (see Figure 3A). In addition, inactivation of ATM sensitized SW480 to SN38 alongside with colibactin (Figure S5G), and olaparib-resistant KP363T and HROC278MET cells, which are characterized by restored HR proficiency as described above, show increased resistance to SN38 (Figure S5H).

Colibactin tolerance discriminates patient-derived organoids with distinct sensitivity profile to SN38

To extend these findings to more translationally relevant models, we exploited a panel of molecularly annotated CRC patient-derived organoids (PDOs). We first implemented a previously reported coculture system[45] and confirmed that this experimental setup was suitable to observe induction of DNA damage in PDOs upon exposure to colibactin (Figure 7A). We then selected a small cohort of PDOs consisting of (1) three models in which sensitivity to SN38 was previously reported (SN38-sensitive patients #2 and #3 and SN38-resistant patient #5, as in Durinikova et al.[33]) and (2) two newly generated PDOs (patients #6 and #7), which proved to be respectively resistant and sensitive to SN38 (Figure 7B). Notably, we found that the three SN38-sensitive models showed significant reduction in cell viability once exposed to colibactin, while SN38-resistant PDOs were unaffected (Figure 7C).

Analysis of *pks* prevalence in CRC patients treated with irinotecan-based regimens

In order to provide initial evidence of the clinical implications of colibactin impact on response to irinotecan-based chemotherapy, we analyzed the *pks* prevalence by endpoint PCR in a retrospective cohort of 40 formalin-fixed paraffin-embedded (FFPE) tumor samples. These were derived from mCRC patients who received FOLFIRI (combination of irinotecan plus 5-fluorouracil), alone or in combination with anti-VEGF treatment as per standard of care. In particular, we collected samples from 20 mCRC patients who had progressive disease as best response to FOLFIRI (defined as "resistant"), and from 20 who had partial response as best response to FOLFIRI (defined as "sensitive"). Given that the entire colibactin genomic sequence is required to synthetize a functional genotoxin, we tested two different amplicons on two different regions of the *pks* island (namely, CLBI and CLBO genes). We considered *pks*-positive those samples in which both amplicons are detected, following a recently published, similar strategy.[46] With this approach, we found 9 of 40 (22.5%) *pks*-positive samples, in accordance with previous results obtained in a published cohort[46] (Figure S6). Interestingly, two samples tested positive for colibactin were derived from a hepatic and a nodal metastasis, suggesting that colibactin might also spread with the tumor outside from primary location. The clinicopathological information for colibactin-positive and colibactin-negative samples is reported in Table S1. We found that 6 of 9 (67%) *pks*-positive patients had progressive disease as best response to FOLFIRI, in contrast with 14 of 31 (45%) in *pks*-negative patients, suggesting a trend toward poorer response to FOLFIRI among *pks*-positive patients.

DISCUSSION

In malignant cancers, DDR pathways are responsible for maintaining the equilibrium between progressive acquisition of driver mutations and avoidance of critical levels of DNA damage. Tumors that harbor genetic defects in DNA repair may reveal a vulnerability to treatments aimed at increasing the DNA damage load.[47] Moreover, the DNA repair status of a tumor may further affect response to chemotherapy.[48] However, how tumors leverage the trade-off between the advantages of increased mutability and the drawbacks of genotoxic susceptibility is still widely unknown. In this regard, compelling evidence supports the involvement of genotoxins from the microbiota.[15,16] Among these, colibactin has been widely studied for its consolidated association with CRC. Although initial evidence has described association of colibactin with clinically relevant features, such as sidedness and overall survival,[17] previous studies failed to find molecular biomarkers which are enriched in colibactin-positive tumors.[13]

Figure 6. Colibactin-tolerant cells show cross-resistance to SN38

(A) Top: waterfall plot showing cell viability of indicated cells 7 days after infection with colibactin at an MOI of 200, normalized on viability of cells infected with empty bacteria. Results represent mean ± SD (n = 2 for MDST8, JVE015, CRC0740XL, and OXCO3; n = 3 for the other cell lines; mean values as in Figure 1B). Bottom: heatmap displaying cell viability after 7 days of treatment with chemotherapeutic agents at clinically relevant, indicated concentrations (data derived from Durinikova et al.[33]).

(B) Viability after colibactin infection at an MOI of 200 (normalized on viability of cells infected with empty bacteria as control) stratifying cells between SN38-sensitive (<35% residual viability after 7 days of treatment) and intermediate-resistant cells. Lines represent mean ± SD. ***$p < 0.001$ (Mann-Whitney test).

(C) Sensitivity to SN38 and oxaliplatin at clinically relevant concentrations in KP363T parental cell line and colibactin-tolerant derivative. Results represent mean ± SD (n = 3). *$p < 0.05$ (Student's t test).

(D) Western blot analysis of replication stress (pRPA and pCHK1) and activation of ATM-CHK2 pathway (pATM and pCHK2) after infection with empty vector or colibactin-producing bacteria, or treatment with SN38 (2 nM) or oxaliplatin (5 μM). NT, untreated (non-infected) cells.

See also Figure S5.

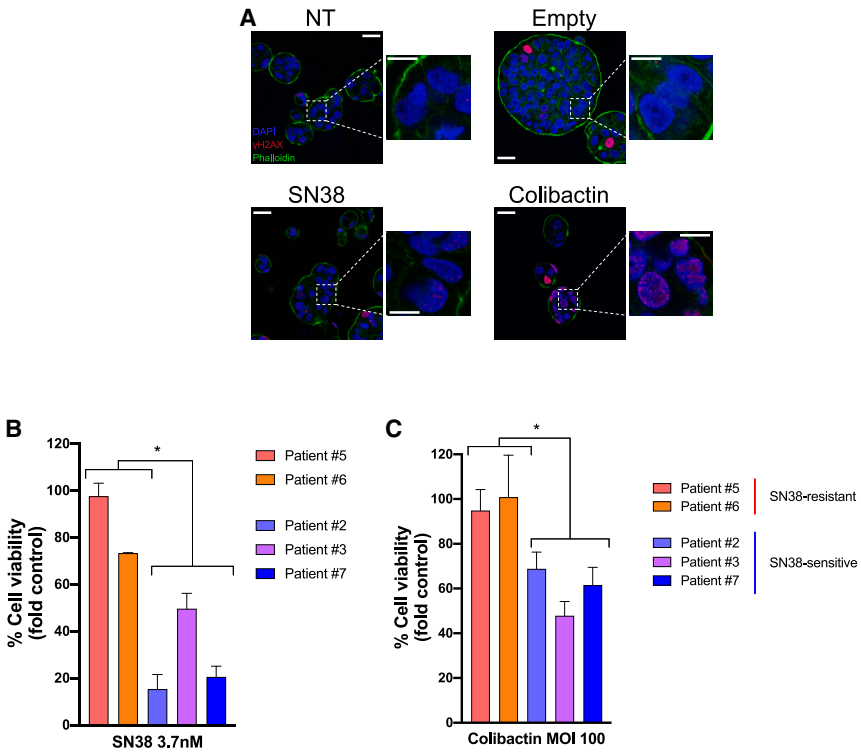

Figure 7. Sensitivity to colibactin correlates with response to SN38 in patient-derived organoids

(A) Representative images of DNA damage induced in patient #5 PDO 24 h after infection with colibactin at an MOI of 100, compared with empty vector control bacteria. NT, untreated (non-infected) cells. SN38 (5 nM) was used as positive control. Scale bar: 25 μm (10 μm in insets).

(B) Sensitivity to SN38 at clinically relevant concentration in PDOs. Data for patients #2, #3, and #5 were reproduced from Durinikova et al.[33] for the purpose of clarity of the figure. Results represent mean ± SD (n = 2). *p < 0.05 (Student's t test).

(C) Viability of indicated PDOs 7 days after infection with colibactin at an MOI of 100, normalized on viability after infection with empty bacteria. Results represent mean ± SD (n = 2). *p < 0.05 (Student's t test).

See also Figure S6.

In our study, we characterized HR proficiency as a key marker of tolerance to colibactin in CRC cells. Previous work described the involvement of different pathways in response to colibactin but relied mainly on artificial modulations of single DNA repair proteins, often in cells of non-colorectal origin. On the contrary, we started from the analysis of the impact of colibactin on a group of ~40 CRC cell lines representative of the molecular heterogeneity of this disease, further mechanistically corroborated by a panel of isogenic cells with genetic inactivation of all the pathways which may be involved in response to colibactin. Moreover, we validated the involvement of the HR pathway by studying different models of HR proficiency restoration.

Colibactin is known to have a pleiotropic effect on the genome of infected cells.[18,21,26] This is recapitulated by our data, as inactivation of *ATM* for DSBs repair, *ATRIP* for RS and *ERCC1* for NER all sensitized cells to colibactin. In parallel, GSEA results showed significantly enriched homology-directed repair pathways among upregulated genes in colibactin-tolerant cells, alongside other DNA repair mechanisms associated with RS response (such as recognition of DNA damage by PCNA-containing replication complex) and NER, paralleling the sensitizing effect obtained with *ATRIP* and *ERCC1* KO, respectively. The involvement of transcription-coupled NER upon colibactin exposure was previously postulated on the basis of colibactin mutational signature profile,[24] while ATR blockade was shown to increase sensitivity to colibactin in previous works.[18] Nevertheless, HR proved to have a prominent role, as inactivation of *ATM* achieved the strongest sensitization phenotype and HR showed the highest NES with GSEA. Indeed, HR may be involved in the repair of DSBs, which are either directly induced by colibactin or result from the induction of RS. Notably, we found that in *ATM*-KO cells the levels of RS increased in parallel to DNA damage. Although colibactin was previously reported to induce activation of *FANCD2*,[18] inactivation of this gene did not result in significant reduction in cell viability upon infection, suggesting that other DDR pathways may rescue cells from cytotoxicity.[49,50] In fact, pharmacological inhibition of ATM was sufficient to sensitize the entire isogenic DDR-KO panel to colibactin, suggesting that ATM provides a salvage mechanism even when other DNA repair pathways activated by colibactin (such as Fanconi anemia and NER) are disabled.

Of translational relevance, we found that HR-deficient cells share a common sensitivity to both colibactin and SN38 but not oxaliplatin. This association retrieved in cells was further confirmed in PDOs models which recapitulated different sensitivity profiles to SN38. In addition, we showed that chronic exposure to colibactin selected for HR proficiency in previously HR-deficient cells, coupled with a resistant phenotype to olaparib and SN38. This provides evidence for the role of colibactin in shaping tumor evolution, suggesting a model in which ongoing mutagenesis driven by a prolonged exposure to colibactin during tumor establishment and progression is capable of selecting a specific DNA repair proficiency phenotype, with implications for further response to treatment. Traditionally, the activity of HR has been associated with response to platinum-based therapies in different tumors.[34] Nevertheless, both colibactin and SN38 may share the exquisite ability to induce DSBs which ultimately activate the HR pathway. Moreover, previous evidence showed that oxaliplatin may induce cancer cell death through several mechanisms which are independent from the capability to induce DNA damage.[51]

Our study poses the preclinical and translational rationale for studying colibactin-producing bacteria as a putative biomarker of resistance to irinotecan-based therapy in the clinical setting.

Given the instability of colibactin, which hampers its direct measurement, current studies mainly rely on detection of the colibactin-encoding *pks* island. In this regard, our analysis of an exploratory cohort of FFPE mCRC samples suggests an enrichment of FOLFIRI-resistant cases in patients with *pks*-positive disease. However, the sole presence of the *pks* island in the tumor at the time of diagnosis may not adequately recapitulate the effect of past exposure to colibactin. Indeed, colibactin-associated mutational signatures have been found in only 5% of CRC patients,[24] in sharp contrast with the prevalence of *pks*$^+$ bacteria in CRCs, estimated to be around 60%.[13] Studies aiming at systematically proving the association of colibactin with clinically relevant outcomes will have to take into consideration different factors, including the specific bacterial strains, the molecular background of the tumor and the impact of past exposure to colibactin in the cancer genome.

In conclusion, our results shed further light on the mode of action of colibactin and its impact on the DNA damage response, and provide additional evidence on the role of this genotoxin in shaping tumor evolution. Future clinical studies will be required to understand whether colibactin can be used as a biomarker of response to chemotherapy to better guide treatment selection in CRC patients.

Limitations of the study

The correlation we found between sensitivity to colibactin and SN38 in PDOs appeared weaker compared with the one observed in cell lines. This may be due to the small number of models analyzed. Furthermore, exposure to colibactin was obtained with an organoid monolayer coculture system, which granted more feasibility and reproducibility, but could have partially affected the genotoxic activity exerted by colibactin.[45] It will be interesting to extended these findings to more models and exploiting more complex coculture systems, such as intraluminal bacterial injections.[45] In addition, given the widespread presence of colibactin in different bacterial strains,[12] and the fact that colibactin mutational signatures were retrieved in different tumors other than those of intestinal origin,[24] it will be fascinating to extend our results to other tumor types. The correlation we retrieved between HR status and sensitivity to colibactin in a small group of ovarian cancer cell lines provides an initial evidence in this regard.

Although we observed a trend toward poorer response to irinotecan-based therapy in *pks*$^+$ mCRC patients, the small cohort size and its retrospective identification represent limitations of our results. Considering the relatively low prevalence of the *pks* island in FFPE samples that we and others observed,[46] assessment of *pks* prevalence in larger and ideally prospective cohorts of patients is warranted to establish the role of colibactin as a potential driver of irinotecan resistance in this clinical setting and assess its impact on patients' survival under treatment.

STAR★METHODS

Detailed methods are provided in the online version of this paper and include the following:

- KEY RESOURCES TABLE
- RESOURCE AVAILABILITY
  - Lead contact
  - Materials availability
  - Data and code availability
- EXPERIMENTAL MODEL AND STUDY PARTICIPANT DETAILS
  - Cell lines
  - Colibactin-producing and empty vector bacteria
  - Patient-derived organoids
  - FFPE tumor samples of CRC patients for analysis of *pks* prevalence
- METHOD DETAILS
  - Bacteria-cell line cocultures
  - Immunofluorescence
  - Colibactin sensitivity and drug proliferation assays
  - Western blot analysis
  - Generation of isogenic DDR knock-out cell lines
  - Generation of olaparib-resistant cell lines
  - Generation of pDRGFP expressing cells
  - Homologous recombination proficiency assay
  - Generation of colibactin-tolerant cell lines
  - RNA extraction and sequencing
  - Gene expression analysis
  - Differential gene expression analysis and GSEA
  - Patient-derived organoids drug screening and bacteria co-cultures
  - Patient-derived organoids immunofluorescence
  - Analysis of *pks* prevalence in FFPE samples of CRC patients
- QUANTIFICATION AND STATISTICAL ANALYSIS

SUPPLEMENTAL INFORMATION

Supplemental information can be found online at https://doi.org/10.1016/j.xcrm.2023.101376.

ACKNOWLEDGMENTS

The research leading to these results has received funding from the European Research Council (ERC) under the European Union's Horizon 2020 research and innovation program (TARGET; grant agreement 101020342) (A.B.); AIRC under 5 per Mille 2018 – ID. 21091 program – principal investigator (PI) A.B., group leaders F.D.N. and L.T.; AIRC under IG 2018 – ID. 21923 project – PI A.B.; International Accelerator Award, ACRCelerate, jointly funded by Cancer Research UK (grants A26825 and A28223), FC AECC (grant GEACC18004-TAB) and AIRC (grant 22795) (A.B. and L.T.); AIRC under Investigator Grant 22802 (L.T.); H2020 grant agreement 754923 COLOSSUS (L.T.); Horizon Europe grant agreement 101058620 canSERV (L.T.); Fondazione Piemontese per la Ricerca sul Cancro-ONLUS, 5x1000 Ministero della Salute 2016 (L.T.); Ricerca Corrente 2023, Italian Ministry of Health (F.D.N.); AIRC under MFAG 2021-ID 26439 project – PI M.R.; AIRC MFAG 2017 ID. 20236 – PI S.A.; AIRC under BRIDGE 2022-ID 27321 –PI S.A.; MIUR Progetti di Ricerca di Rilevante Interesse Nazionale (PRIN) Bando 2022 under the project "A Comprehensive Analysis of Dietary Risk Factors, Colibactin and Tumor Molecular Features in Early-Onset Colorectal Cancer" (grant 2022LSFKWE) (A.S.-B. and S.A.). A.S. was supported by the AIRC "Professoressa Fiamma Nicolodi" Postdoc Fellowship for Italy (project code 28518). E.M. was supported by the FIRC-AIRC "Michele e Carlo Ardizzone" fellowship for Italy. G.M. is a PhD student within the European School of Molecular Medicine (SEMM). The authors wish to thank V. Costanzo and F. D'Adda di Fagagna (IFOM ETS [the AIRC Institute of Molecular Oncology], Milan, Italy) for their critical reading of the manuscript and insightful suggestions. The authors also thank

members of the Bardelli lab at the University of Torino and at IFOM for scientific support and critical reading of the article.

AUTHOR CONTRIBUTIONS

Conceptualization, A.S. and A.B.; formal analysis, A.S., E.R., G.G., and G.M.; investigation, A.S., E.R., G.G., E.M., N.M.R., S.L., E.P., and M.R.; funding acquisition, M.R., S.A., L.T., F.D.N., and A.B.; methodology, A.S., E.R., G.G., E.M., L.T., M.D., F.D.N., and A.B.; visualization, A.S., E.R., G.G., and E.M.; resources, N.M.R., S.L., G.M., E.D., P.P.V., A.L., M.A., M.R., S.A., A.S.-B., E.B., M.C.A., S.S., L.T., M.D., F.D.N., and A.B.; supervision, A.B.; writing – original draft, A.S., E.R., and A.B.; writing – review & editing, A.S., E.R., G.G., E.M., N.M.R., S.L., G.M., E.D., A.L., M.A., E.P., M.R., S.A., L.T., M.D., F.D.N., and A.B.

DECLARATION OF INTERESTS

The authors declare the following competing interests, which are unrelated to the results of the study. A.B. reports receiving commercial research grants from Neophore, AstraZeneca, and Boehringer; he is an advisory board member/unpaid consultant for Inivata and Neophore, holds ownership interest in Neophore, and is an advisory board member/consultant for Illumina, Guardant Health, Inivata, and Roche/Genentech Global CRC. F.D.N. received honoraria from Pierre Fabre. L.T. has received research grants from Menarini, Merck KGaA, Merus, Pfizer, Servier, and Symphogen. S.A. acted as consultant for MSD Italia outside the submitted work and has a patent (102022000007535) pending. A.S.-B. is an advisory board member for Amgen, Bayer, Novartis, Pierre Fabre, and Servier. S.S. is an advisory board member for Agenus, AstraZeneca, Bayer, Bristol Myers Squibb, CheckmAb, Daiichi Sankyo, Guardant Health, Menarini, Merck, Novartis, Roche-Genentech, and Seagen.

Received: April 16, 2023
Revised: November 8, 2023
Accepted: December 15, 2023
Published: January 15, 2024

REFERENCES

1. Wong, S.H., and Yu, J. (2019). Gut microbiota in colorectal cancer: mechanisms of action and clinical applications. Nat. Rev. Gastroenterol. Hepatol. *16*, 690–704.
2. Andrei, P., Battuello, P., Grasso, G., Rovera, E., Tesio, N., and Bardelli, A. (2022). Integrated approaches for precision oncology in colorectal cancer: The more you know, the better. Semin. Cancer Biol. *84*, 199–213.
3. Hanahan, D. (2022). Hallmarks of Cancer: New Dimensions. Cancer Discov. *12*, 31–46.
4. Thomas, A.M., Manghi, P., Asnicar, F., Pasolli, E., Armanini, F., Zolfo, M., Beghini, F., Manara, S., Karcher, N., Pozzi, C., et al. (2019). Metagenomic analysis of colorectal cancer datasets identifies cross-cohort microbial diagnostic signatures and a link with choline degradation. Nat. Med. *25*, 667–678.
5. Wirbel, J., Pyl, P.T., Kartal, E., Zych, K., Kashani, A., Milanese, A., Fleck, J.S., Voigt, A.Y., Palleja, A., Ponnudurai, R., et al. (2019). Meta-analysis of fecal metagenomes reveals global microbial signatures that are specific for colorectal cancer. Nat. Med. *25*, 679–689.
6. Tilg, H., Adolph, T.E., Gerner, R.R., and Moschen, A.R. (2018). The Intestinal Microbiota in Colorectal Cancer. Cancer Cell *33*, 954–964.
7. Bertocchi, A., Carloni, S., Ravenda, P.S., Bertalot, G., Spadoni, I., Lo Cascio, A., Gandini, S., Lizier, M., Braga, D., Asnicar, F., et al. (2021). Gut vascular barrier impairment leads to intestinal bacteria dissemination and colorectal cancer metastasis to liver. Cancer Cell *39*, 708–724.e11.
8. Geller, L.T., Barzily-Rokni, M., Danino, T., Jonas, O.H., Shental, N., Nejman, D., Gavert, N., Zwang, Y., Cooper, Z.A., Shee, K., et al. (2017). Potential role of intratumor bacteria in mediating tumor resistance to the chemotherapeutic drug gemcitabine. Science *357*, 1156–1160.
9. LaCourse, K.D., Zepeda-Rivera, M., Kempchinsky, A.G., Baryiames, A., Minot, S.S., Johnston, C.D., and Bullman, S. (2022). The cancer chemotherapeutic 5-fluorouracil is a potent Fusobacterium nucleatum inhibitor and its activity is modified by intratumoral microbiota. Cell Rep. *41*, 111625.
10. Yu, T., Guo, F., Yu, Y., Sun, T., Ma, D., Han, J., Qian, Y., Kryczek, I., Sun, D., Nagarsheth, N., et al. (2017). Fusobacterium nucleatum Promotes Chemoresistance to Colorectal Cancer by Modulating Autophagy. Cell *170*, 548–563.e16.
11. Barrett, M., Hand, C.K., Shanahan, F., Murphy, T., and O'Toole, P.W. (2020). Mutagenesis by Microbe: the Role of the Microbiota in Shaping the Cancer Genome. Trends Cancer *6*, 277–287.
12. Chagneau, C.V., Payros, D., Tang-Fichaux, M., Auvray, F., Nougayrède, J.P., and Oswald, E. (2022). The pks island: a bacterial Swiss army knife?: Colibactin: beyond DNA damage and cancer. Trends Microbiol. *30*, 1146–1159.
13. Gaab, M.E., Lozano, P.O., Ibañez, D., Manese, K.D., Riego, F.M., Tiongco, R.E., and Albano, P.M. (2022). A Meta-Analysis on the Association of Colibactin-Producing pks+ Escherichia coli with the Development of Colorectal Cancer. Lab. Med. *54*, 75–82.
14. Arima, K., Zhong, R., Ugai, T., Zhao, M., Haruki, K., Akimoto, N., Lau, M.C., Okadome, K., Mehta, R.S., Väyrynen, J.P., et al. (2022). Western-Style Diet, pks Island-Carrying Escherichia coli, and Colorectal Cancer: Analyses From Two Large Prospective Cohort Studies. Gastroenterology *163*, 862–874.
15. Arthur, J.C., Perez-Chanona, E., Mühlbauer, M., Tomkovich, S., Uronis, J.M., Fan, T.J., Campbell, B.J., Abujamel, T., Dogan, B., Rogers, A.B., et al. (2012). Intestinal inflammation targets cancer-inducing activity of the microbiota. Science *338*, 120–123.
16. Dejea, C.M., Fathi, P., Craig, J.M., Boleij, A., Taddese, R., Geis, A.L., Wu, X., DeStefano Shields, C.E., Hechenbleikner, E.M., Huso, D.L., et al. (2018). Patients with familial adenomatous polyposis harbor colonic biofilms containing tumorigenic bacteria. Science *359*, 592–597.
17. Georgeson, P., Steinfelder, R.S., Harrison, T.A., Pope, B.J., Zaidi, S.H., Qu, C., Lin, Y., Joo, J.E., Mahmood, K., Clendenning, M., et al. (2023). Genotoxic colibactin mutational signature in colorectal cancer is associated with clinicopathological features, specific genomic alterations and better survival. Preprint at medRxiv.
18. Bossuet-Greif, N., Vignard, J., Taieb, F., Mirey, G., Dubois, D., Petit, C., Oswald, E., and Nougayrède, J.P. (2018). The Colibactin Genotoxin Generates DNA Interstrand Cross-Links in Infected Cells. mBio *9*. e02393–17.
19. Xue, M., Kim, C.S., Healy, A.R., Wernke, K.M., Wang, Z., Frischling, M.C., Shine, E.E., Wang, W., Herzon, S.B., and Crawford, J.M. (2019). Structure elucidation of colibactin and its DNA cross-links. Science *365*, eaax2685.
20. Wilson, M.R., Jiang, Y., Villalta, P.W., Stornetta, A., Boudreau, P.D., Carrá, A., Brennan, C.A., Chun, E., Ngo, L., Samson, L.D., et al. (2019). The human gut bacterial genotoxin colibactin alkylates DNA. Science *363*, eaar7785.
21. Nougayrède, J.P., Homburg, S., Taieb, F., Boury, M., Brzuszkiewicz, E., Gottschalk, G., Buchrieser, C., Hacker, J., Dobrindt, U., and Oswald, E. (2006). Escherichia coli induces DNA double-strand breaks in eukaryotic cells. Science *313*, 848–851.
22. Cuevas-Ramos, G., Petit, C.R., Marcq, I., Boury, M., Oswald, E., and Nougayrède, J.P. (2010). Escherichia coli induces DNA damage in vivo and triggers genomic instability in mammalian cells. Proc. Natl. Acad. Sci. USA *107*, 11537–11542.
23. Iftekhar, A., Berger, H., Bouznad, N., Heuberger, J., Boccellato, F., Dobrindt, U., Hermeking, H., Sigal, M., and Meyer, T.F. (2021). Genomic aberrations after short-term exposure to colibactin-producing E. coli transform primary colon epithelial cells. Nat. Commun. *12*, 1003.
24. Pleguezuelos-Manzano, C., Puschhof, J., Huber, A.R., van Hoeck, A., Wood, H.M., Nomburg, J., Gurjao, C., Manders, F., Dalmasso, G., Stege,

P.B., et al. (2020). Mutational signature in colorectal cancer caused by genotoxic pks. Nature.

25. Xue, M., Wernke, K.M., and Herzon, S.B. (2020). Depurination of Colibactin-Derived Interstrand Cross-Links. Biochemistry *59*, 892–900.
26. Nougayrède, J.P., Chagneau, C.V., Motta, J.P., Bossuet-Greif, N., Belloy, M., Taieb, F., Gratadoux, J.J., Thomas, M., Langella, P., and Oswald, E. (2021). A Toxic Friend: Genotoxic and Mutagenic Activity of the Probiotic Strain Escherichia coli Nissle 1917. mSphere *6*, e0062421.
27. Ngoi, N.Y.L., Pham, M.M., Tan, D.S.P., and Yap, T.A. (2021). Targeting the replication stress response through synthetic lethal strategies in cancer medicine. Trends Cancer *7*, 930–957.
28. Nickoloff, J.A., Sharma, N., Taylor, L., Allen, S.J., and Hromas, R. (2021). The Safe Path at the Fork: Ensuring Replication-Associated DNA Double-Strand Breaks are Repaired by Homologous Recombination. Front. Genet. *12*, 748033.
29. Balmus, G., Pilger, D., Coates, J., Demir, M., Sczaniecka-Clift, M., Barros, A.C., Woods, M., Fu, B., Yang, F., Chen, E., et al. (2019). ATM orchestrates the DNA-damage response to counter toxic non-homologous end-joining at broken replication forks. Nat. Commun. *10*, 87.
30. Ait Saada, A., Lambert, S.A.E., and Carr, A.M. (2018). Preserving replication fork integrity and competence via the homologous recombination pathway. DNA Repair *71*, 135–147.
31. Cong, K., and Cantor, S.B. (2022). Exploiting replication gaps for cancer therapy. Mol. Cell *82*, 2363–2369.
32. Medico, E., Russo, M., Picco, G., Cancelliere, C., Valtorta, E., Corti, G., Buscarino, M., Isella, C., Lamba, S., Martinoglio, B., et al. (2015). The molecular landscape of colorectal cancer cell lines unveils clinically actionable kinase targets. Nat. Commun. *6*, 7002.
33. Durinikova, E., Reilly, N.M., Buzo, K., Mariella, E., Chilà, R., Lorenzato, A., Dias, J.M.L., Grasso, G., Pisati, F., Lamba, S., et al. (2022). Targeting the DNA Damage Response Pathways and Replication Stress in Colorectal Cancer. Clin. Cancer Res. *28*, 3874–3889.
34. Arena, S., Corti, G., Durinikova, E., Montone, M., Reilly, N.M., Russo, M., Lorenzato, A., Arcella, P., Lazzari, L., Rospo, G., et al. (2020). A Subset of Colorectal Cancers with Cross-Sensitivity to Olaparib and Oxaliplatin. Clin. Cancer Res. *26*, 1372–1384.
35. Sharma, A., Singh, K., and Almasan, A. (2012). Histone H2AX phosphorylation: a marker for DNA damage. Methods Mol. Biol. *920*, 613–626.
36. Ngoi, N.Y.L., Westin, S.N., and Yap, T.A. (2022). Targeting the DNA damage response beyond poly(ADP-ribose) polymerase inhibitors: novel agents and rational combinations. Curr. Opin. Oncol. *34*, 559–569.
37. Rodrigue, A., Lafrance, M., Gauthier, M.C., McDonald, D., Hendzel, M., West, S.C., Jasin, M., and Masson, J.Y. (2006). Interplay between human DNA repair proteins at a unique double-strand break in vivo. EMBO J. *25*, 222–231.
38. Lord, C.J., and Ashworth, A. (2016). BRCAness revisited. Nat. Rev. Cancer *16*, 110–120.
39. Xu, J., Shen, Y., Wang, C., Tang, S., Hong, S., Lu, W., Xie, X., and Cheng, X. (2021). Arsenic compound sensitizes homologous recombination proficient ovarian cancer to PARP inhibitors. Cell Death Discov. *7*, 259.
40. Bradbury, A., O'Donnell, R., Drew, Y., Curtin, N.J., and Sharma Saha, S. (2020). Characterisation of Ovarian Cancer Cell Line NIH-OVCAR3 and Implications of Genomic, Transcriptomic, Proteomic and Functional DNA Damage Response Biomarkers for Therapeutic Targeting. Cancers *12*, 1939.
41. Mateo, J., Lord, C.J., Serra, V., Tutt, A., Balmaña, J., Castroviejo-Bermejo, M., Cruz, C., Oaknin, A., Kaye, S.B., and de Bono, J.S. (2019). A decade of clinical development of PARP inhibitors in perspective. Ann. Oncol. *30*, 1437–1447.
42. Pierce, A.J., Johnson, R.D., Thompson, L.H., and Jasin, M. (1999). XRCC3 promotes homology-directed repair of DNA damage in mammalian cells. Genes Dev. *13*, 2633–2638.
43. Gillespie, M., Jassal, B., Stephan, R., Milacic, M., Rothfels, K., Senff-Ribeiro, A., Griss, J., Sevilla, C., Matthews, L., Gong, C., et al. (2022). The reactome pathway knowledgebase 2022. Nucleic Acids Res. *50*, D687–D692.
44. Cervantes, A., Adam, R., Roselló, S., Arnold, D., Normanno, N., Taïeb, J., Seligmann, J., De Baere, T., Osterlund, P., Yoshino, T., et al. (2022). Metastatic colorectal cancer: ESMO Clinical Practice Guideline for diagnosis, treatment and follow-up. Ann. Oncol.
45. Puschhof, J., Pleguezuelos-Manzano, C., Martinez-Silgado, A., Akkerman, N., Saftien, A., Boot, C., de Waal, A., Beumer, J., Dutta, D., Heo, I., and Clevers, H. (2021). Intestinal organoid cocultures with microbes. Nat. Protoc. *16*, 4633–4649.
46. Villariba-Tolentino, C., Cariño, A.M., Notarte, K.I., Macaranas, I., Fellizar, A., Tomas, R.C., Angeles, L.M., Abanilla, L., Lim, A., Aguilar, M.K.C., and Albano, P.M. (2021). pks(+) Escherichia coli more prevalent in benign than malignant colorectal tumors. Mol. Biol. Rep. *48*, 5451–5458.
47. Pilié, P.G., Tang, C., Mills, G.B., and Yap, T.A. (2019). State-of-the-art strategies for targeting the DNA damage response in cancer. Nat. Rev. Clin. Oncol. *16*, 81–104.
48. Reilly, N.M., Novara, L., Di Nicolantonio, F., and Bardelli, A. (2019). Exploiting DNA repair defects in colorectal cancer. Mol. Oncol. *13*, 681–700.
49. Michl, J., Zimmer, J., and Tarsounas, M. (2016). Interplay between Fanconi anemia and homologous recombination pathways in genome integrity. EMBO J. *35*, 909–923.
50. Li, N., Wang, J., Wallace, S.S., Chen, J., Zhou, J., and D'Andrea, A.D. (2020). Cooperation of the NEIL3 and Fanconi anemia/BRCA pathways in interstrand crosslink repair. Nucleic Acids Res. *48*, 3014–3028.
51. Bruno, P.M., Liu, Y., Park, G.Y., Murai, J., Koch, C.E., Eisen, T.J., Pritchard, J.R., Pommier, Y., Lippard, S.J., and Hemann, M.T. (2017). A subset of platinum-containing chemotherapeutic agents kills cells by inducing ribosome biogenesis stress. Nat. Med. *23*, 461–471.
52. Leto, S.M., Ferri, M., Sassi, F., Zanella, E.R., Cottino, F., Vurchio, V., Catalano, I., Ferrero, A., Zingaretti, C.C., Marchiò, C., et al. (2023). Synthetic lethal interaction with BCL-XL blockade deepens response to cetuximab in patient-derived models of metastatic colorectal cancer. Clin. Cancer Res. *29*, 1102–1113.
53. Bossuet-Greif, N., Belloy, M., Boury, M., Oswald, E., and Nougayrede, J.-P. (2017). Protocol for HeLa Cells Infection with Escherichia coli Strains Producing Colibactin and Quantification of the Induced DNA-damage. Bio. Protoc. *7*, e2520.
54. Sanjana, N.E., Shalem, O., and Zhang, F. (2014). Improved vectors and genome-wide libraries for CRISPR screening. Nat. Methods *11*, 783–784.
55. Wang, K., Singh, D., Zeng, Z., Coleman, S.J., Huang, Y., Savich, G.L., He, X., Mieczkowski, P., Grimm, S.A., Perou, C.M., et al. (2010). MapSplice: accurate mapping of RNA-seq reads for splice junction discovery. Nucleic Acids Res. *38*, e178.
56. Li, B., and Dewey, C.N. (2011). RSEM: accurate transcript quantification from RNA-Seq data with or without a reference genome. BMC Bioinf. *12*, 323.
57. Love, M.I., Huber, W., and Anders, S. (2014). Moderated estimation of fold change and dispersion for RNA-seq data with DESeq2. Genome Biol. *15*, 550.
58. Gennady, K., Vladimir, S., Nikolay, B., Boris, S., Maxim, N.A., and Alexey, S. (2021). Fast Gene Set Enrichment Analysis. Preprint at bioRxiv *888*. 060012.

STAR★METHODS

KEY RESOURCES TABLE

REAGENT or RESOURCE	SOURCE	IDENTIFIER
Antibodies		
Rabbit anti-gamma-H2AX Antibody, Affinity Purified	Bethyl	Cat# A300-081A; RRID:AB_203288
Anti-RAD51	Millipore	Cat# ABE257; RRID:AB_10850319
Donkey Anti-Rabbit IgG (H + L) Polyclonal Antibody, Alexa Fluor 555 Conjugated	Molecular Probes	Cat# A-31572; RRID:AB_162543
Donkey anti-Mouse IgG (H + L) ReadyProbes Secondary Antibody, Alexa Fluor™ 488	Thermo Fisher Scientific	Cat# R37114; RRID:AB_2556542
Phospho-Histone H2A.X (Ser139) (D7T2V) Mouse mAb	Cell Signaling Technology	Cat# 80312; RRID:AB_2799949
Histone H2A.X (D17A3) XP Rabbit mAb	Cell Signaling Technology	Cat# 7631; RRID:AB_10860771
Anti-Vinculin, clone V284	Millipore	Cat# 05–386; RRID:AB_11212640
ATM (phospho S1981) antibody [EP1890Y]	Abcam	Cat# ab81292; RRID:AB_1640207
Rabbit Anti-ATM Monoclonal Antibody, Unconjugated, Clone D2E2	Cell Signaling Technology	Cat# 2873; RRID:AB_2062659
Rabbit anti-Phospho RPA32 (S33) Antibody, Affinity Purified	Bethyl	Cat# A300-246A; RRID:AB_2180847
Recombinant Anti-RPA32/RPA2 antibody [4E4]	Abcam	Cat# ab252861; RRID:AB_292764
Rad51C (2H11)	Santa Cruz Biotechnology	Cat# sc-56214; RRID:AB_2238197
Phospho-Chk1 (Ser345) (133D3) Rabbit mAb	Cell Signaling Technology	Cat# 2348; RRID:AB_331212
Chk1 (2G1D5) Mouse mAb	Cell Signaling Technology	Cat# 2360; RRID:AB_2080320
Phospho-Chk2 (Thr68) (C13C1) Rabbit mAb	Cell Signaling Technology	Cat# 2197; RRID:AB_2080501
Mouse Anti-Chk2 Monoclonal Antibody, Unconjugated, Clone 1C12	Cell Signaling Technology	Cat# 3440; RRID:AB_2229490
ATRIP Antibody	Cell Signaling Technology	Cat# 2737, RRID:AB_823659
FANCD2 Antibody - BSA Free	Novus Biologicals	Cat# NB100-182, RRID:AB_10002867
ERCC1 (D61F5) Rabbit mAb	Cell Signaling Technology	Cat# 5437, RRID:AB_10831838
REV1 Antibody (A-11)	Santa Cruz Biotechnology	Cat# sc-393022, RRID:AB_2885169
Bacterial and virus strains		
Escherichia coli DH10B pBeloBAC empty vector	Prof. Jean Philippe Nougayrede[21]	N/A
Escherichia coli DH10B pBeloBAC-pks	Prof. Jean Philippe Nougayrede[21]	N/A
Chemicals, peptides, and recombinant proteins		
DAPI (4′,6-diamidino-2-phenylindole, dihydrochloride)	Thermo Scientific	Cat# 62247
Fetal Bovine Serum (South America) Sterile Filtered	Euroclone	Cat# ECS0180L
L-Glutamine solution	Sigma-Aldrich	Cat# G7513
Antibiotic Antimycotic Solution (100×), Stabilized	Sigma-Aldrich	Cat# A5955
Trypsin-EDTA Solution	Sigma-Aldrich	Cat# T3924
Crystal Violet Solution	Sigma-Aldrich	Cat# V5265-500ML
Oxaliplatin	MedChemExpress	Cat# HY-17371
SN38	MedChemExpress	Cat# HY-13704
Olaparib	MedChemExpress	Cat# HY-10162
AZD0156	MedChemExpress	Cat# HY-100016
Critical commercial assays		
Venor®GeM Classic	Minerva Biolabs	Cat# 11-1250
PowerPlex® 16 HS System	Promega	Cat# DC2100

(*Continued on next page*)

Continued

REAGENT or RESOURCE	SOURCE	IDENTIFIER
Pierce™ BCA Protein Assay Kit	Thermo Scientific	Cat# 23225
Western Blotting Amersham™ ECL™ Prime	Cytica	Cat# RPN2236
Lipofectamine™ 3000 Transfection Reagent	Invitrogen	Cat# L3000001
NEBNext® High-Fidelity 2X PCR Master Mix	New England Biolabs GmbH	Cat# M0541S
CellTiter-Glo® Luminescent Cell Viability Assay	Promega	Cat# G7573
Maxwell® RSC DNA FFPE Kit	Promega	Cat# AS1450
Deposited data		
RNA-Seq data	This study	ENA:PRJEB68048
Experimental models: Cell lines		
Human: COGA-5 cell line	Laboratory of L.A. Huber	RRID:CVCL_A076
Human: DLD-1 cell line	ATCC	RRID:CVCL_0248
Human: HCT 116 cell line	NCI60	RRID:CVCL_0291
Human: OUMS-23 cell line	JCRB	RRID:CVCL_3088
Human: WiDr cell line	Laboratory of R. Bernards	RRID:CVCL_2760
Human: SW480 cell line	ATCC	RRID:CVCL_0546
Human: DiFi cell line	Laboratory of J. Baselga	RRID:CVCL_6895
Human: HT29 cell line	NCI60	RRID:CVCL_A8EZ
Human: HROC183 cell line	Laboratory of M. Linnebacher	RRID:CVCL_1D16
Human: Co-115 cell line	Laboratory of R. Hamelin	RRID:CVCL_D102
Human: SNU-977 cell line	KCLB	RRID:CVCL_5109
Human: HROC284Met cell line	Laboratory of M. Linnebacher	RRID:CVCL_1U91
Human: MDST8 cell line	ECACC	RRID:CVCL_2588
Human: GEO cell line	Laboratory of G. Tortora	RRID:CVCL_0271
Human: KM20 cell line	KCLB	RRID:CVCL_L095
Human: KM12 cell line	NCI60	RRID:CVCL_1331
Human: RW-7213 cell line	Laboratory of D. Arango	RRID:CVCL_D175
Human: SNU-1411 cell line	KCLB	RRID:CVCL_5025
Human: LS411N cell line	ATCC	RRID:CVCL_1385
Human: LS1034 cell line	ATCC	RRID:CVCL_1382
Human: VACO 432 cell line	Labboratory of B. Vogelstein	RRID:CVCL_5402
Human: HCC2998 cell line	NCI60	RRID:CVCL_1266
Human: CL-11 cell line	DSMZ	RRID:CVCL_1978
Human: HROC69 cell line	Laboratory of M. Linnebacher	RRID:CVCL_1G06
Human: JVE015 cell line	LUMC	RRID:CVCL_EG16
Human: CRC0174_XL cell line	Lead contact	N/A
Human: SK-CO-1 cell line	ATCC	RRID:CVCL_0626
Human: HROC131 T0 M3 cell line	Laboratory of M. Linnebacher	RRID:CVCL_1D13
Human: HDC-114 cell line	Laboratory of M. Schwab	RRID:CVCL_A376
Human: SW1116 cell line	ATCC	RRID:CVCL_0544
Human: CRC0740_XL cell line	Lead contact	N/A
Human: SNU-61 cell line	KCLB	RRID:CVCL_5078
Human: HROC59 cell line	Laboratory of M. Linnebacher	RRID:CVCL_1G04
Human: HROC39 cell line	Laboratory of M. Linnebacher	RRID:CVCL_1U81
Human: C106 cell line	ECACC	RRID:CVCL_M011
Human: OX-CO-3 cell line	Laboratory of V. Cerundolo	RRID:CVCL_B452
Human: HROC278Met T2 M2 cell line	Laboratory of M. Linnebacher	RRID:CVCL_1U90
Human: NCI-H498 cell line	ATCC	RRID:CVCL_1563
Human: KP363T cell line	LUMC	RRID:CVCL_EG34

(*Continued on next page*)

Continued

REAGENT or RESOURCE	SOURCE	IDENTIFIER
Human: SW480 *ATM* KO cell line	This study	N/A
Human: SW480 *ATRIP* KO cell line	This study	N/A
Human: SW480 *ERCC1* KO cell line	This study	N/A
Human: SW480 *FANCD2* KO cell line	This study	N/A
Human: SW480 *REV1* KO cell line	This study	N/A
Human: A2780 cell line	ECACC	RRID:CVCL_0134
Human: UWB1.289 cell line	ATCC	RRID:CVCL_B079
Human: UWB1.289+*BRCA1* cell line	ATCC	RRID:CVCL_B078
Human: KP363T olaparib-resistant cell line	This study	N/A
Human: HROC278MET olaparib-resistant cell line	This study	N/A
Human: KP363T colibactin-tolerant cell line	This study	N/A
Human: KP363T empty long term cell line	This study	N/A
Human: HROC39 colibactin-tolerant cell line	This study	N/A
Oligonucleotides		
sgRNA targeting *ATM* 5′- CCAAGGCTATTCAGTG TGCG-3′	Durinikova et al.[33]	N/A
sgRNA targeting *ATRIP* 5′-GCGAGACTCACTACA TCAGA-3′	This study	N/A
sgRNA targeting *ERCC1* 5′-GCTCTGTGTAGATCG GAATA-3′	This study	N/A
sgRNA targeting *FANCD2* 5′-AAGAAGACTGTCAA AATCTG-3′	This study	N/A
sgRNA targeting *REV1* 5′-AAACTAATGATGTTGC ATGG-3′	This study	N/A
CLBI forward primer 5′-CGCTTCATCAACACGC TTTA-3′	This study	N/A
CLBI reverse primer 5′-GCAAAAACCGGCTACT TGTC-3′	This study	N/A
CLBO forward primer 5′-CGTCGTTATTTACCGC ACCT-3′	This study	N/A
CLBO reverse primer 5′-CACTACGCGACCAAGA CAGA-3′	This study	N/A
Recombinant DNA		
Plasmid: pDRGFP	Addgene	RRID:Addgene_26475
Plasmid: pCBASceI	Addgene	RRID:Addgene_26477
Plasmid: lentiCRISPR v2	Addgene	RRID:Addgene_52961
Software and algorithms		
GeneMapper® Software v.6	Applied Biosystems	RRID:SCR_014290
GraphPad Prism v.8	GraphPad	RRID:SCR_002798
ImageJ v1.53a	https://ImageJ.nih.gov/ij/	N/A
MapSplice v2.2.1	http://www.netlab.uky.edu/p/bioinfo/	http://www.netlab.uky.edu/p/bioinfo/
Samtools v1.14	https://samtools.sourceforge.net/	https://samtools.sourceforge.net/
Ubu 1.2	UNC-Chapel Hill Bioinformatics Utilities	https://github.com/mozack/ubu/blob/master/src/main/java/edu/unc/bioinf/ubu/Ubu.java
Rsem v1.3.3	https://github.com/deweylab/RSEM	https://github.com/deweylab/RSEM
R v4.1	The R Foundation for Statistical Computing	https://www.R-project.org/
Tximport	Bioconductor	https://bioconductor.org/packages/release/bioc/html/tximport.html
Deseq2	Bioconductor	https://bioconductor.org/packages/release/bioc/html/DESeq2.html

(*Continued on next page*)

Continued

REAGENT or RESOURCE	SOURCE	IDENTIFIER
fGSEA	Bioconductor	https://bioconductor.org/packages/release/bioc/html/fgsea.html
ggplot2 v3.3	Tidyverse	https://ggplot2.tidyverse.org

RESOURCE AVAILABILITY

Lead contact

Further information and requests for resources and reagents should be directed to and will be fulfilled by the lead contact, prof. Alberto Bardelli (alberto.bardelli@unito.it).

Materials availability

Isogenic SW480 DDR knock-out cell lines, KP363T and HROC278MET olaparib-resistant cells, KP363T and HROC39 colibactin-tolerant cells and KP363T re-infected with empty vector bacteria are available from the lead contact (A.B.) under a Material Transfer Agreement.

Data and code availability

(1) RNA-seq data obtained for KP363T cells with acquired tolerance to colibactin or exposed to empty vector bacteria for the same number of infections were deposited in the European Nucleotide Archive (ENA:PRJEB68048). Other raw data reported in this paper will be shared by the lead contact upon request.
(2) This paper does not report original code.
(3) Any additional information required to reanalyze the data reported in this paper is available from the lead contact upon request.

EXPERIMENTAL MODEL AND STUDY PARTICIPANT DETAILS

Cell lines

Each cell line was cultured in its specific medium, routinely supplemented with 10% fetal bovine serum (FBS), 2 mM L-glutamine and antibiotics (100 U/ml of penicillin and 100 mg/mL of streptomycin), and grown at 37°C on a 5% CO_2 air incubator. Cells were routinely screened for absence of Mycoplasma contamination using the Venor GeM Classic kit (Minerva Biolabs). All the cell lines used were confirmed negative for Mycoplasma contamination in all the tests performed. The identity of each cell line was checked no more than 3 months before performing the experiments using the PowerPlex 16 HS System (Promega), through short tandem repeat tests at 16 different loci (D5S818, D13S317, D7S820, D16S539, D21S11, vWA, TH01, TPOX, CSF1PO, D18S51, D3S1358, D8S1179, FGA, Penta D, Penta E and amelogenin). Amplicons from multiplex PCRs were separated by capillary electrophoresis (3730 DNA Analyzer, Applied Biosystems) and analyzed using GeneMapper v.3.7 software (Life Technologies). Short tandem repeat results for all the CRC cell lines matched the profiles previously published.[32] The origin of all the CRC cell lines used in the present study was previously reported.[32,33] A2780 cell line was obtained from ECACC. UWB1.289 parental and +BRCA1 derivative cells were obtained from ATCC.

Colibactin-producing and empty vector bacteria

Escherichia coli DH10B strains harboring a Bacterial Artificial Chromosome (pBeloBAC) with the pks island and their counterpart with corresponding empty-vector BAC were kindly provided by Jean-Philippe Nougayède, Université de Toulouse, France.[21]

Patient-derived organoids

Regarding PDOs #2, #3 and #5, tumor samples were obtained from patients treated at Niguarda Cancer Center (Milan, Italy) after written consent and the study was conducted in accordance with the local Independent Ethical Committee (protocol 194/2010). PDOs establishment was previously reported.[34] For PDOs #6 and #7, samples were procured and the study was conducted under the approval of the Review Board of the Candiolo Cancer Institute (PROFILING protocol No. 001-IRCC-00IIS-10), and all patients provided informed consent. PDOs #6 and #7 were established as previously described.[52] Organoids were tested for Mycoplasma and maintained at 37°C in a humidified atmosphere of 5% CO2. All the PDOs were cultured in Cultrex Basement Membrane Extract (BME) Type 2 (Amsbio) with ENAS medium. ENAS medium was prepared starting from Basal Medium (consisting of advanced DMEM/F12 medium containing 100 U/mL penicillin, 100 μg/mL streptomycin, 2 mmol/L GlutaMAX, 10 mmol/L HEPES and 50μg/mL primocin) supplemented with: 1 × B27 supplement (Invitrogen), 1 × N2 supplement (Invitrogen), 1.25 mmol/L N-acetyl-cysteine (Sigma Aldrich), 10 mmol/L nicotinamide (Sigma Aldrich), 10 nmol/L gastrin (Sigma), 50 ng/mL human EGF (Life Technologies), 100 ng/mL Noggin (PeproTech), 500 nmol/L TGFb type I receptor inhibitor A83-01 (Tocris), and 10 μmol/L p38 MAPK inhibitor SB202190 (Sigma Aldrich).

FFPE tumor samples of CRC patients for analysis of *pks* prevalence

Forty metastatic CRC patients treated with FOLFIRI alone or in combination with an anti-VEGFR agent (as per standard-of-care) were retrospectively identified at Grande Ospedale Metropolitano Niguarda, Milan, Italy. All patients were enrolled within the AlfaOmega Master Observational Trial (NCT04120935) and signed a dedicated informed consent. Patients were identified and considered eligible for this study based on their response to FOLFIRI as follow: 20 who had partial response ('sensitive'), and 20 who had progressive disease ('resistant') as best response to FOLFIRI administered as per standard of care. Electronic charts records were reviewed to collect and analyze patients' clinicopathological features.

METHOD DETAILS

Bacteria-cell line cocultures

Infections with colibactin-producing or empty-vector bacteria were performed as previously described.[53] Briefly, on day 0 cancer cells were plated at different densities based on the experimental designs described below, and a bacterial overnight culture in Luria Bertani (LB) broth, supplemented with 25μg/mL chloramphenicol as selection marker, was started. The following day, 0.5mL of overnight cultures were added to 9.5mL of Dulbecco's Modified Eagle Medium with high glucose (DMEM, Sigma Aldrich) supplemented with 25mM HEPES, and allowed to grow for 2 h, during which bacteria reached exponential phase growth (infection medium). Optical density at 600nm (OD600) was measured to monitor growth, and a conversion factor from OD600 to CFU/mL was previously assessed in our experimental conditions. Plated cancer cells were carefully washed with PBS to remove antibiotics, and infection medium diluted in DMEM 25mM HEPES was added to achieve the desired multiplicity-of-infection (MOI), in a volume of interaction medium of 1mL for 6-multiwell plates (used for Western Blot) and 200μL for 24-multiwell plates (used for colibactin sensitivity assays and immunofluorescence analysis). Bacteria-cancer cells cocultures were then incubated at 37°C for 4 h. After that, cells were carefully washed with PBS supplemented with 20μg/mL gentamicin to remove remaining bacteria and complete medium with gentamicin was added. Cells were then incubated until analysis.

Immunofluorescence

Cell lines were plated on glass coverslips at a density of 8×10^4 per coverslip. The following day, cells were either infected with colibactin-producing or empty-vector bacteria or treated with indicated chemotherapy. Cells were then fixed at indicated timepoints. For irradiation, cells were grown on glass coverslips (2×10^5 cells per well) in a 24-well plate. Twenty-four hours after plating, cells were exposed to ionizing radiation and allowed to recover for 4 h, followed by fixation. Cells were fixed in 4% paraformaldehyde for 20 min at room temperature (RT) and permeabilized with 0.1% Triton X-100 for 5 min on ice. Then, cells were treated with BSA 1% for 1 h at RT, followed by overnight incubation at +4°C with the following primary antibodies diluted in PBS containing 1% of donkey serum: anti-phospho-Histone H2AX (Ser139) rabbit monoclonal antibody (Bethyl Laboratories A700-053) (1:600); anti-RAD51 (Millipore ABE257; 1:100). After washing, cells were fluorescently labeled with an Alexa Fluor 555 or Alexa Fluor 488 donkey anti-rabbit antibody (Molecular Probes; 1:400) for 1 h at room temperature. Nuclei were stained with DAPI. Slides were then mounted using the fluorescence mounting medium (Dako). For quantification of γH2AX and RAD51 nuclear foci, nuclei were detected with a Leica DMI6000B fluorescence microscope (Leica Microsystems) under a 40× dry objective using the Leica Application Suite Advanced Fluorescence software (v.2.6.3.8173). Images were captured at 10 individual z-planes and were merged using the "Z Project" function in ImageJ. Individual nuclei were scored for foci positivity, identified based on signal intensity above general background staining levels and presence within the nucleus as assessed by concomitant DAPI staining. Cells containing ≥5 distinct foci were defined as foci-positive, and the percentage of positive nuclei was calculated as [(number of RAD51 foci-positive nuclei)/(number of nuclei scored)]* 100.[34] Doubling of RAD51 foci-positive nuclei in cells infected with colibactin-producing bacteria compared with empty vector bacteria, or in irradiated cells compared with untreated controls, was considered as threshold of positivity, in accordance with previously published analysis of post-irradiation RAD51 foci.[34] Representative images shown were acquired with a confocal laser scanning microscope (TCS SPE II, Leica), using the Leica Application Suite Advanced Fluorescence software (v.2.6.3.8173), and processed with Adobe Photoshop CS5.

Colibactin sensitivity and drug proliferation assays

On day 0, cells were plated at different densities in 24-multiwell plates. For colibactin sensitivity assay, the following day cells were infected with colibactin-producing or empty-vector bacteria at indicated MOIs as described above. Following 4 h of infection, residual bacteria were removed and cells were incubated at 37°C 5% CO_2 for 7 days in their respective complete medium supplemented with 20μg/mL gentamicin. For drug proliferation assays, serial dilutions of each drug were added to the cells, which were then incubated at 37°C in 5% CO_2 for 7 days. Following incubation, cells were fixed with 4% paraformaldehyde and stained with 1% Crystal Violet-Methanol solution (Sigma-Aldrich). Crystal Violet was then solubilized with 10% acetic acid and absorbance was quantified at 595nm. Oxaliplatin (S1224), SN-38 (S4908), olaparib (AZD2281, Ku-0059436, S1060), and ATM inhibitor AZD0156 were purchased from MedChemExpress. The sensitivity profile to chemotherapeutic agents shown in Figure 6A was derived from ref. [33].

Western blot analysis

On day 0, cells were plated at different densities in 6-multiwell plates. The following day, cells were infected with colibactin and empty bacteria at indicated MOIs as described above. total cellular proteins were extracted by solubilizing cells in boiling SDS buffer (50 mM

Tris-HCl [pH 7.5], 150 mM NaCl, and 1% SDS). Samples were boiled for 5 min at 95°C and sonicated for 10 s. Extracts were clarified by centrifugation and normalized with the BCA Protein Assay Reagent kit (Thermo). Western blot detection was performed with enhanced chemiluminescence system (GE Healthcare) and peroxidase conjugated secondary antibodies (Amersham). Detection of the chemiluminescent signal was performed with ChemiDoc Imaging System (Bio-Rad). The following primary antibodies were used for western blotting: anti-Vinculin (MERCK 05–386; 1:3,000); anti-HSP90 (Santa Cruz Biotechnology, sc-13119; 1:1,000); anti-actin (Santa Cruz Biotechnology; 1:3,000); anti-phospo-H2AX (Ser139) (Cell Signaling Technology, 80312S; 1:1,000); anti-H2AX (Cell Signaling Technology, 7631S; 1:1,000); anti-phospho-ATM (Ser1981) (Abcam, ab81292; 1:1,000); anti-ATM (Cell Signaling Technology, 2873S; 1:1,000); anti-phospho-RPA32 (Ser33) (Bethyl Laboratories A300-246A; 1:1,000); anti-RPA32 (Abcam, ab252861; 1:2,000); anti-RAD51C (Santa Cruz Biotechnology, sc-56214; 1:1,000); anti-phospho-CHK1 (S345) (Cell Signaling Technology, 2348S; 1:1,000); anti-CHK1 (Cell Signaling Technology, 2360S; 1:1,000); anti-phospho-CHK2 (Cell Signaling Technology, 2197S; 1:1,000); anti-CHK2 (Cell Signaling Technology, 3440S, 1:1000).

Generation of isogenic DDR knock-out cell lines

Generation of ATM-KO SW480 was previously reported.[33] To generate the DDR gene panel knock-outs, we used the genome editing one vector system (lentiCRISPR-v2). Small guide RNAs (sgRNAs) were designed using the CRISPR tool (http://crispr.mit.edu). Annealed sgRNAs oligonucleotides targeting the human DDR genes were cloned into BsmbI lentiCRISPR-v2 plasmid, as previously described.[54] In order to reduce the risk of mutagenesis from off-target effects, we exploited transient expression of Cas9 and sgRNA through transfection. Using SW480 cells, transfection was carried out using Lipofectamine 3000 (Life technologies) and OptiMEM (Invitrogen), according to the manufacturer's instructions. After 48 h, cells were incubated with puromycin (Sigma Aldrich) for 4 days and subsequently single cell diluted in 96-well plates. Several clones were selected for each DDR gene knock-out and loss of DDR proteins expression were confirmed by Western blot. Plasmid lentiCRISPR v2 was a gift from Feng Zhang (Addgene plasmid # 52961).

Generation of olaparib-resistant cell lines

KP363T and HROC278MET olaparib-resistant derivatives were obtained treating parental (sensitive[34]) cells with 5 μM of olaparib for several months, until resistant derivatives emerged. Resistance to olaparib was confirmed with drug screening comparing to parental counterparts.

Generation of pDRGFP expressing cells

Cells were seeded at a density of 2.5×10^5 cells/well in 6-multiwell plates. The following day, cells were transfected with pDRGFP plasmid using Lipofectamine 3000 (Life technologies) following manufacturer's instruction. pDRGFP plasmid is composed of two differentially mutated GFP (green fluorescent protein) genes oriented as direct repeats and separated by a drug selection marker.[42] One of the GFP genes is mutated to contain the recognition site for the Sce-I endonuclease and, as a result, will undergo a DSB when Sce-I is ectopically expressed.[42] A homologous recombination event between the two GFP genes results in the expression of intact GFP protein. Seventy-two hours after infection, puromycin (Sigma Aldrich) was used to select stably pDRGFP-expressing cells. Generation of pDRGFP-expressing KP363T parental cells was previously reported.[34] pDRGFP was a gift from Maria Jasin (Addgene plasmid # 26475).

Homologous recombination proficiency assay

The pDRGFP-expressing cells were seeded at a density of 2.5×10^5 cells/well in 6-multiwell plates. The following day, cells were transfected with the Sce-I-expressing plasmid (pCBASce-I)[42] using Lipofectamine 3000 following manufacturer's instruction. Fifty to 60 h after transfection, cells were harvested and analyzed by flow cytometry using the Beckman Coulter CyAn ADP analyzer with the Summit v.4.3 software. pCBASceI was a gift from Maria Jasin (Addgene plasmid # 26477).

Generation of colibactin-tolerant cell lines

KP363T and HROC39 colibactin-tolerant cell derivatives (and KP363T control cells re-exposed to empty-vector bacteria) were obtained through longitudinal re-infections with colibactin-producing bacteria. At the beginning of the experiment, 5 million cells were plated in a T75 tissue flask for each condition. The following day, cells were infected with colibactin-producing or empty vector bacteria at MOI 100. Each week, cells were detached, counted (in order to be able to calculate the MOI) and re-plated in a new T75 flask. Cells were then infected the following day. When cells were too few to be detached, they were left recovering for an additional week before reinfection. For cell re-infected with empty vector bacteria, since they kept growing exponentially, when detached only 5 million cells were re-plated for each reinfection.

RNA extraction and sequencing

Total RNA was extracted using the Maxwell RSC miRNA Tissue Kit (AS1460, Promega). The quantification of RNA was performed by Thermo Scientific Nanodrop 1000 (Agilent) and Qubit 3.0 Fluorometer (Life Technologies). RNA integrity was evaluated with the Agilent 2100 Bioanalyzer using the Agilent RNA 6000 Nano Kit. Total RNA (800 ng) with RNA integrity number (RIN) score between 9 and 10 was used as input to the Illumina TruSeq RNA Sample Prep Kit v2-Set B (48Rxn), according to the manufacturer's protocol. After

library preparation, sequencing was performed on NextSeq500 to get single-end 150 bp reads. Three biologically independent RNA samples were extracted and sequenced for both KP363T colibactin-tolerant cells and counterpart cells exposed to long-term treatment with the empty bacteria.

Gene expression analysis

RNA-seq reads were initially aligned to hg38 using the splice-aware MapSplice tool.[55] The resulting BAM files underwent processing via ubu sam-xlate and sam-filter to translate genomic coordinates into transcriptomic ones and to exclude reads with indels, large inserts and zero mapping quality. Then, the quantification of transcripts and genes was conducted using RSEM[56] and GENCODE v33 as gene annotation. Starting from the RSEM-derived gene results (expected counts and effective lengths), robust FPKM values were subsequently calculated, using the tximport R Bioconductor package and the fpkm function included in the DESeq2 R Bioconductor package.[57] Finally, the robust FPKM values were log2-transformed, the gene expression matrix was annotated with gene names from the GENCODE annotation file and genes of interest were selected to calculate the z-scores.

Differential gene expression analysis and GSEA

RSEM-derived gene results were used to perform differential gene expression analysis exploiting the tximport and DESeq2 R Bioconductor packages.[57] KP363T colibactin-tolerant cells (alternative condition) were compared with KP363T cells exposed to long-term treatment with the empty bacteria (reference condition). Independent filtering was performed as implemented by the results function and adjusted p values were obtained by applying the Benjamini–Hochberg (BH) method. In addition, the lfcShrink function was used to shrink the log2 fold changes. Genes were annotated with gene names from the GENCODE annotation file and those whose adjusted p value was <5% were considered as differentially expressed.

We subsequently performed pre-ranked GSEA with the fgsea function from the fGSEA R Bioconductor package.[58] Genes were ranked based on the obtained shrunken log2 fold changes. The enrichment analysis was performed considering different categories of genes involved in DNA repair. Specifically, three groups of gene sets were derived from the Reactome database[43] (Reactome:R-HSA-73894; https://reactome.org/content/detail/R-HSA-73894) in the following way: the 7 main DNA-repair Pathways were selected as 'Level 1' gene sets, all their branches were selected as 'Level 2' gene sets and all the branches derived from Level 2 were selected as 'Level 3' gene sets. Each level was analyzed independently from the others and for each gene set we obtained the BH-adjusted p value, the normalized enrichment score (NES) and the list of genes in the leading edge.

Patient-derived organoids drug screening and bacteria co-cultures

Sensitivity to SN38 in PDOs #2, #3 and #5 was derived from the ref. [33]. In order to screen the sensitivity to SN38 in PDO #6 and #7, following previously published protocols,[33] organoids were enzymatically dissociated using TrypLE Express Enzyme for 10 to 20 min at 37°C to obtain single-cell suspensions and seeded at a density of 7,000–8,000 cells per well in 96-well plates precoated with BME Type 2 and overlayed with 100 μL of growth media containing 1% BME. The treatment with drugs started on day 2 after seeding when 3D structures were visible. Organoids were treated in fresh 150 μL medium containing 2% BME with increasing doses of SN-38 in technical triplicates, covering physiologic concentrations of the drug. Treatment was done automatically by Tecan D300e Digital Dispenser. MG-132 at 4 μmol/L concentration was used as a positive control; DMSO served as a negative control.

For PDO-bacteria cocultures, PDOs were dissociated and plated as described above in the complete absence of antibiotics. Infection with colibactin-producing or empty-vector bacteria was performed on day 2 after seeding following a previously published protocol for PDOs plated on BME-coated plates.[45] Briefly, PDOs were washed twice with PBS before adding overnight bacterial cultures diluted in infection medium (DMEM-high glucose with 25mM HEPES as described above) at desired MOI. Bacteria-PDOs cocultures were incubated at 37°C for 3 h. After that, cells were carefully washed with PBS with 20μg/mL gentamicin to remove remaining bacteria and ENAS medium supplemented with cell-permeable antibiotic primocin. MG-132 at 4 μmol/L concentration was used as a positive control, while infection with empty vector bacteria served as negative control.

The viability was assayed at the end of the experiment after 7 days from infection or treatment administration by CellTiter-Glo Luminescent Cell Viability assay (Promega) with modifications. Briefly, plates were equilibrated at room temperature for 30 min and reagent was mixed 1:1 with organoid media in the wells. Organoids were then subjected to the lysis by vigorous shaking for 25 min, and readout was done by plate reader Tecan SPARK 10M. The raw CellTiter-Glo values were normalized to the mean of the negative control wells on a per-plate basis. The control wells (positive and negative) were used to calculate Z factors to indicate the quality of the data generated in the screening plate, as described before.[33]

Patient-derived organoids immunofluorescence

Treated or infected organoids, grown on chamber slides (Falcon 8-well Culture Slide) previously precoated with BME, were fixed in 4% paraformaldehyde in PBS solution for 30 min at room temperature and permeabilized with 0.5% Triton X-100 in PBS for 30 min at room temperature. Organoids were then incubated with 1% BSA in PBS for 60 min, followed by incubation overnight with anti-phospho-Histone H2AX (Ser139; Bethyl Laboratories A300-081A; 1:600) primary antibody diluted in PBS containing 1% of BSA and 1% of donkey serum. After washing, organoids were fluorescently labeled with Alexa Fluor 488 donkey anti-rabbit antibody (Invitrogen)

diluted 1:400 in PBS containing 1% BSA and 1% donkey serum for 1 to 2 h. Nuclei were stained with DAPI and F-actin with Alexa Fluor 555 phalloidin (50 μg/mL). Slides were then mounted using the fluorescence mounting medium (Dako) and analyzed using a confocal laser scanning microscope (TCS SPE II, Leica).

Analysis of *pks* prevalence in FFPE samples of CRC patients

DNA from 3 formalin-fixed paraffin-embedded (FFPE) tissue slides of 10μm thickness was extracted with the Maxwell RSC DNA FFPE Kit (AS1450, Promega). Amplicons of the *CLBI* and *CLBO* genes (132bp and 60bp, respectively) of the *pks* genomic island were obtained with the NEBNext High-Fidelity 2X PCR Master Mix (M0541S; New England Biolabs GmbH) and resolved through electrophoresis on 2% agarose gel with 10,000x SYBR Safe DNA gel stain (S33102; Invitrogen). Detection of signal was performed with ChemiDoc Imaging System (Bio-Rad). DNA extracted from colibactin-producing *E.coli* and water were used as positive and negative controls, respectively.

QUANTIFICATION AND STATISTICAL ANALYSIS

Statistical details for each experiment are specified in the corresponding figure legends. Statistical significance was determined by unpaired Student's *t* test, Mann-Whitney test, one-way ANOVA or two-way ANOVA (GraphPad Prism) as specified for each experiment and $p < 0.05$ was considered statistically significant.

Cell Reports Medicine, Volume *5*

Supplemental information

Tolerance to colibactin correlates with homologous recombination proficiency and resistance to irinotecan in colorectal cancer cells

Alberto Sogari, Emanuele Rovera, Gaia Grasso, Elisa Mariella, Nicole Megan Reilly, Simona Lamba, Gianluca Mauri, Erika Durinikova, Pietro Paolo Vitiello, Annalisa Lorenzato, Marco Avolio, Eleonora Piumatti, Emanuela Bonoldi, Maria Costanza Aquilano, Sabrina Arena, Andrea Sartore-Bianchi, Salvatore Siena, Livio Trusolino, Manuela Donalisio, Mariangela Russo, Federica Di Nicolantonio, David Lembo, and Alberto Bardelli

Supplemental figures

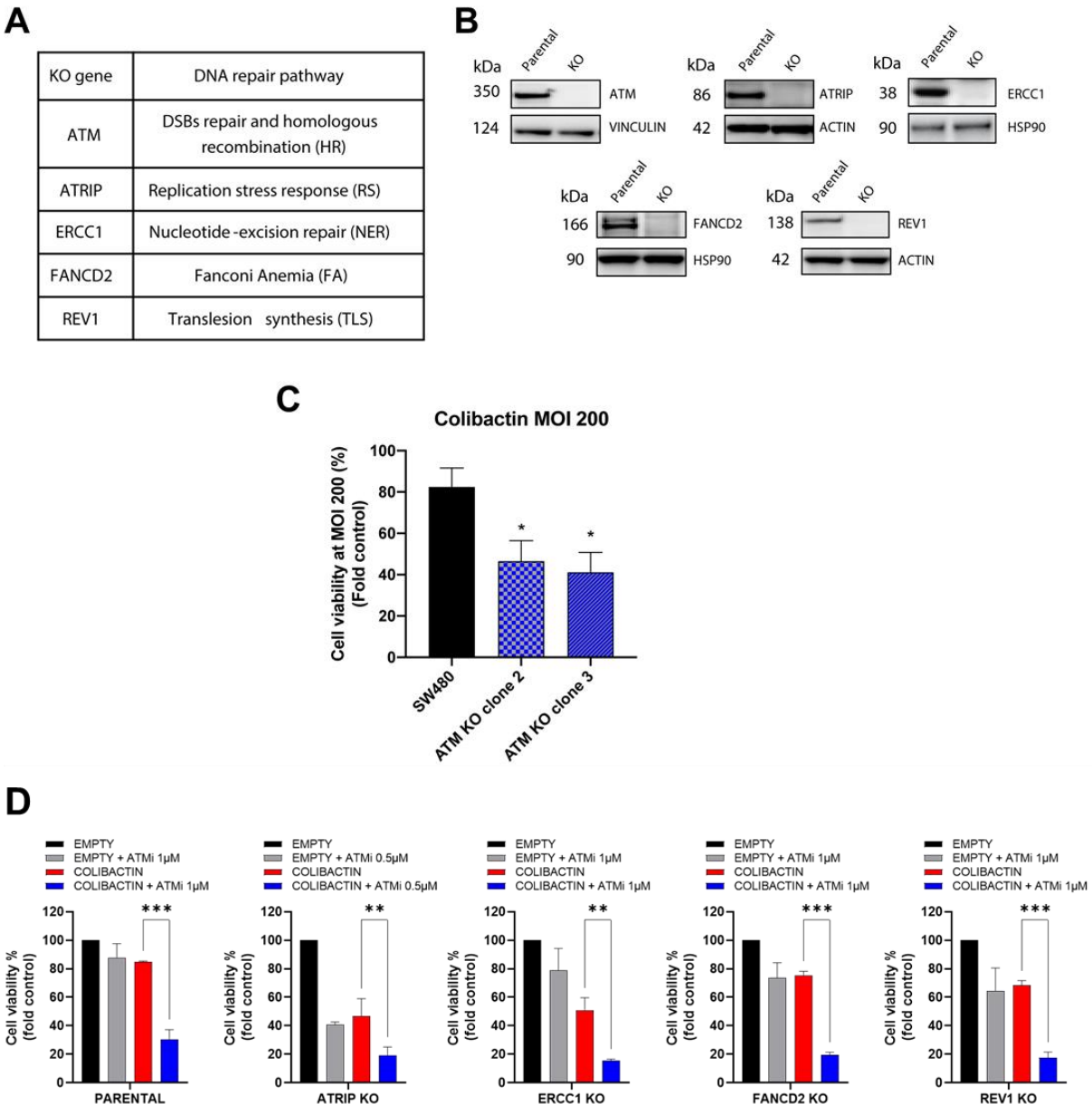

Figure S1. Genetic inactivation of *ATM* sensitizes cells to colibactin. (**A**) Gene targets and corresponding DNA repair pathways inactivated with CRISPR/Cas9 technology in SW480 isogenic cell lines. (**B**) Western blot analysis validating genetic inactivation of indicated DDR protein by CRISPR/Cas9. (**C**) Cell viability of SW480 parental cells and two additional *ATM*-KO isogenic cells 7 days after infection with colibactin at MOI 200, normalized on viability after infection with empty bacteria. Results represent mean ± SD (n=3). *: $p<0.05$ (Student's t test, compared to parental SW480). Data on SW480 parental cells as in Figure 2A. (**D**) Cell viability of SW480 parental and isogenic DDR KO cells in the presence or absence of ATM inhibitor (ATMi) AZD0156. Results represent mean ± SD (n=3). **: $p<0.01$; ***: $p<0.001$ (one-way ANOVA with Bonferroni's multiple comparisons test). Related to Figure 2.

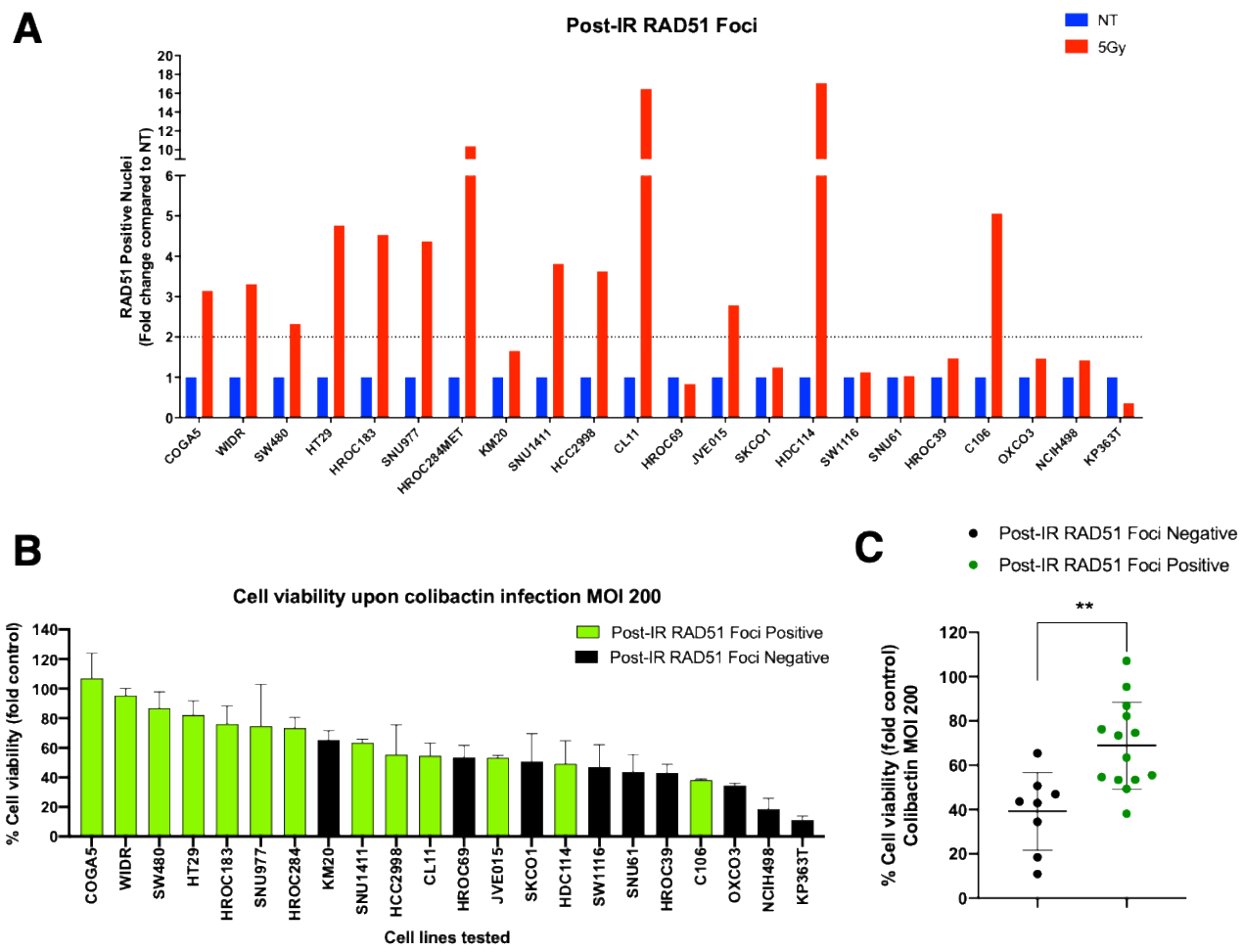

Figure S2. Homologous recombination deficient cell lines show increased sensitivity to colibactin. (**A**) Quantification of RAD51 nuclear foci in indicated cells after exposure to ionizing radiations 5Gy, normalized on untreated (NT) controls. Nuclei with five or more foci were scored as positive, and at least 500 nuclei were counted for each sample. Doubling of RAD51-positive cells after irradiation compared to untreated controls was considered as threshold to define RAD51-positive cells. Results on COGA5, HCC2998, HROC69, SKCO1, HROC39, OXCO3 and KP363T are reproduced from reference (34) for the purpose of clarity of the Figure. (**B**) Waterfall plot showing cell viability of indicated cells 7 days after infection with colibactin at MOI 200, normalized on viability of cells infected with empty bacteria as control, stratified based on post-IR RAD51 positivity as marker of HR proficiency. Results represent mean ± SD (n=3; mean values as in fig. 1B). (**C**) Viability after colibactin infection at MOI 200 (normalized on viability of cells infected with empty bacteria as control) stratifying cells between RAD51 foci-positive and negative. *: $p<0.05$ (Mann Whitney test). Related to Figure 3.

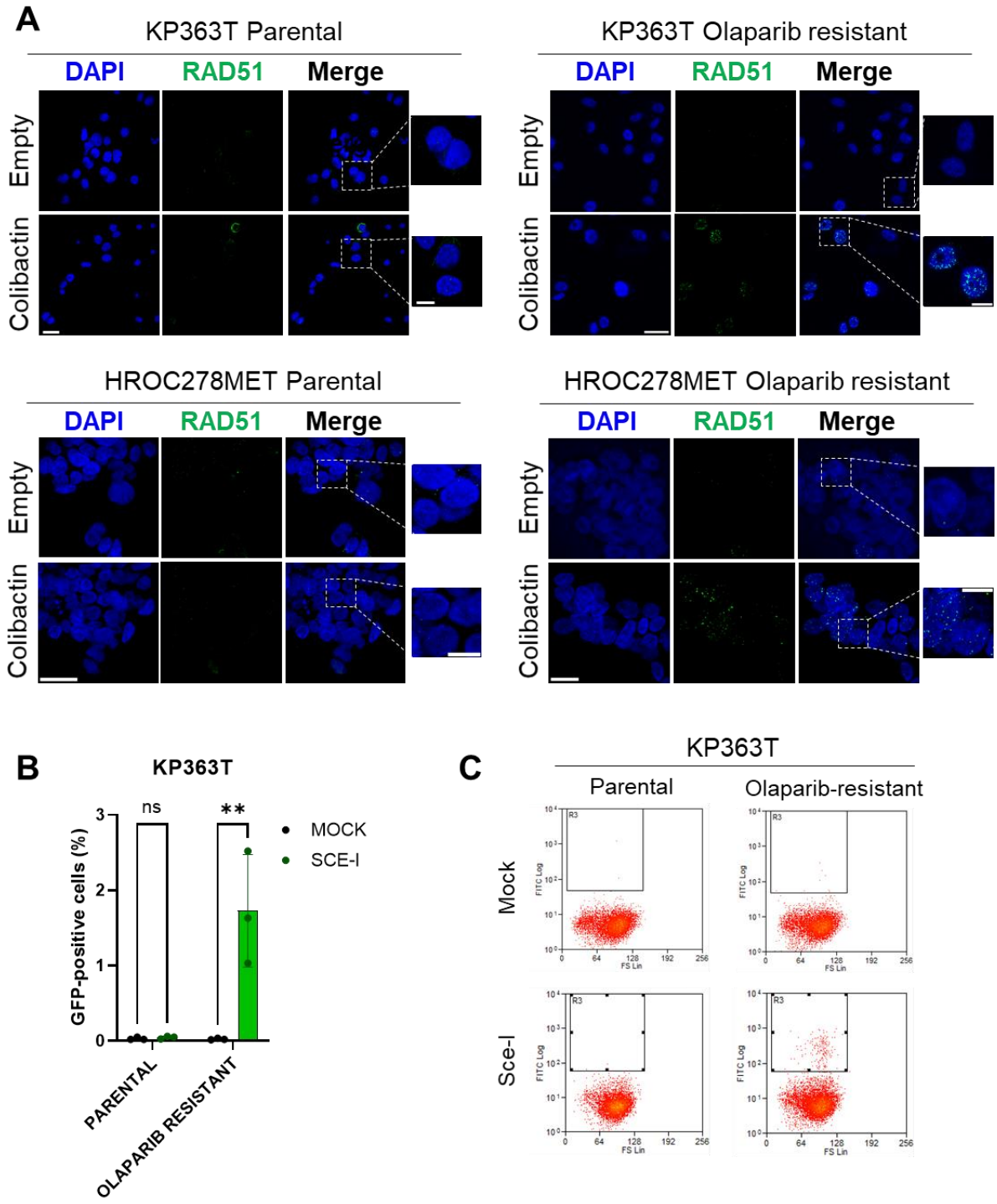

Figure S3. Restoration of HR proficiency in olaparib-resistant cells. (**A**) Percentage of GFP-positive cells in KP363T parental cells and olaparib resistant counterpart transfection with mock or pCBASce-I (Sce-I) plasmid. Results represent mean ± SD (n=3). **: p<0.01 (two-way ANOVA with Bonferroni's multiple tests correction). Ns, not statistically significant. (**B**) Representative flow cytometric acquisition of cells analyzed in panel A. (**C**) Representative images of RAD51 foci 24 hours after infection of indicated cells with colibactin or empty bacteria at MOI 200. Scale bar: 25µm (10µm in insets). Related to Figure 4.

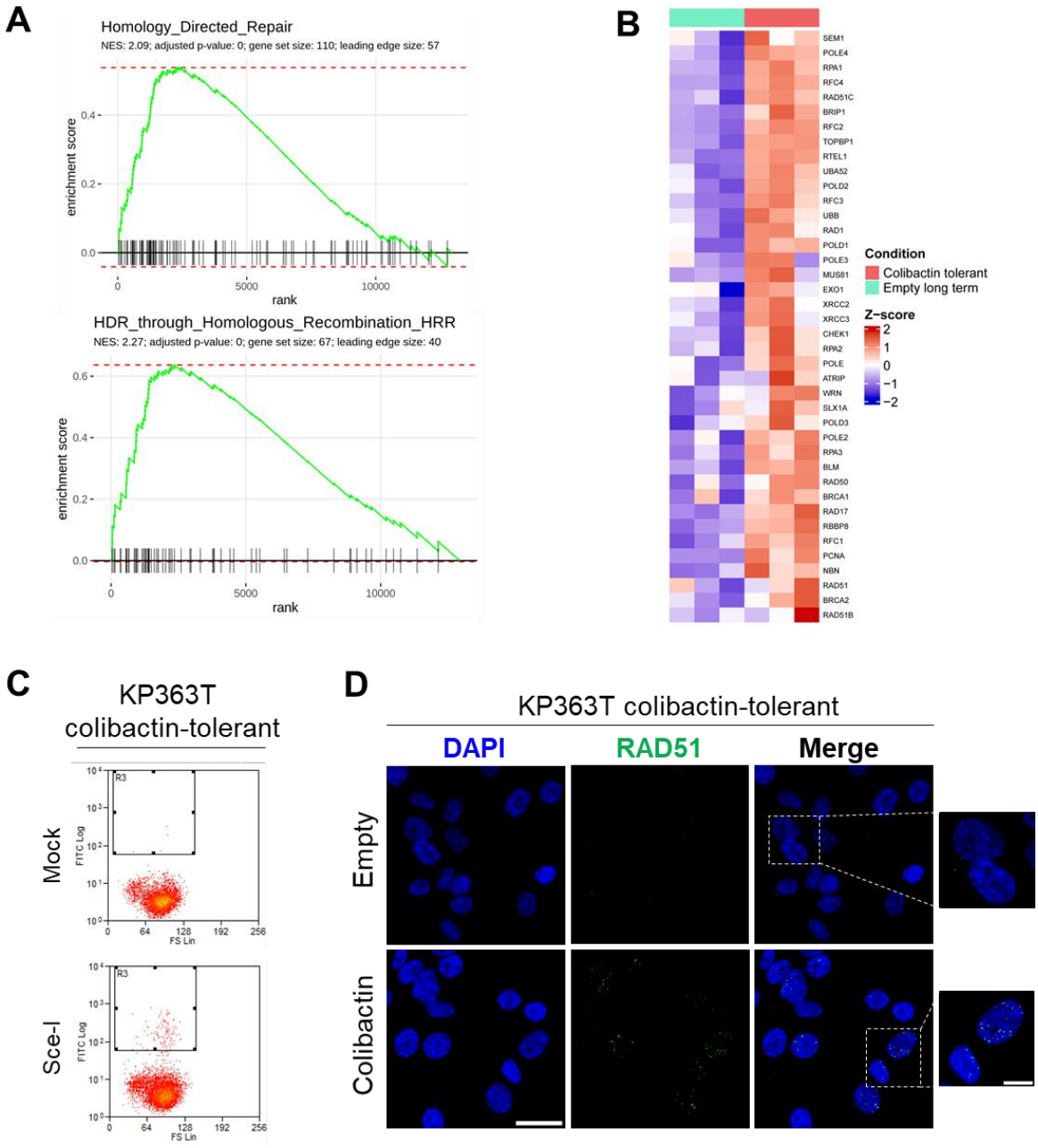

Figure S4. Restoration of HR proficiency in KP363T colibactin-tolerant cells. (**A**) Gene set enrichment analysis (GSEA) for 'Homology_Directed_Repair' (Level 2) and 'HDR_through_Homologous_Recombination_HRR' (Level 3). (**B**) Heatmap of z-scores of $\log_2$(FPKM+1) values of the leading edge genes of 'HDR_through_Homologous_Recombination_HRR' in the Level 3 of Reactome gene set. (**C**) KP363T colibactin-tolerant cells, stably expressing pDRGFP, were transfected with the pCBASce-I plasmid and analyzed by flow cytometry. Results of one representative experiment are reported. (**D**) Representative images of RAD51 foci 24 hours after infection of indicated cells with colibactin or empty bacteria at MOI 200. Scale bar: 25µm (10µm in insets). Related to Figure 5.

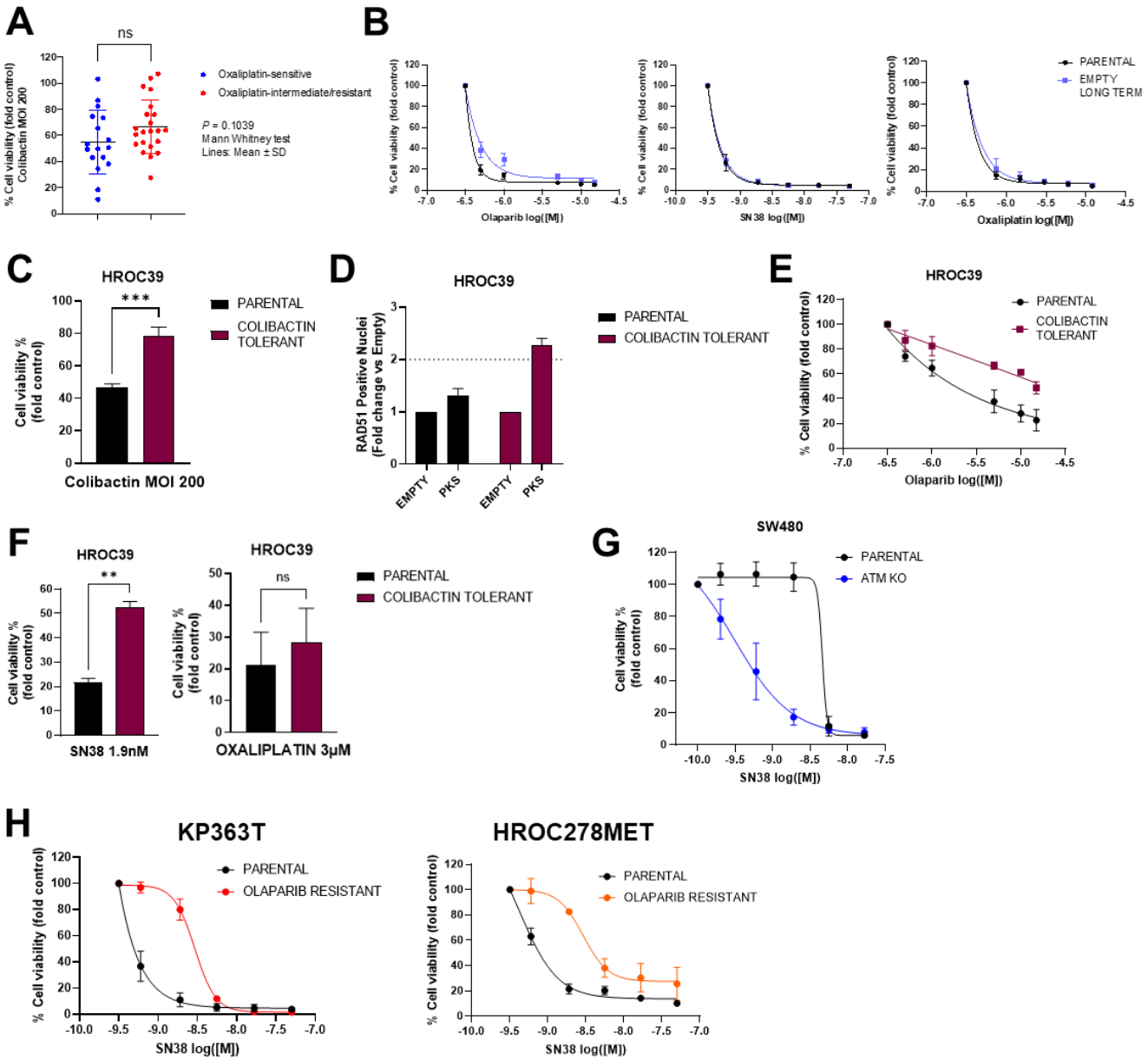

Figure S5. Colibactin selects a HR-proficient, irinotecan-resistant phenotype. (**A**) Viability after infection with colibactin at MOI 200 (normalized on viability of cells infected with empty bacteria as control) stratifying cells between oxaliplatin-sensitive (<35% residual viability after 7 days of treatment) and intermediate-resistant cells. Ns, not statistically significant (Mann Whitney test). (**B**) Sensitivity to olaparib (left panel), SN38 (middle panel) and oxaliplatin (right panel) of KP363T parental and corresponding derivative cells which were long-term longitudinally re-infected with empty-vector bacteria. Results represent mean ± SD (n=2). (**C**) Cell viability of HROC39 parental cells and colibactin-tolerant derivative 7 days after infection with colibactin, normalized on viability after infection with empty bacteria. Results represent mean ± SD (n=3). ***: $p<0.001$ (Student's t test). (**D**) Quantification of nuclear RAD51 foci in HROC39 parental cells and colibactin-tolerant derivative 24 hours after infection, normalized on exposure to empty bacteria. Results represent mean ± SD (n=2). (**E**) Sensitivity to olaparib in HROC39 parental cell line and colibactin-tolerant derivative. Results represent mean ± SD (n=2). (**F**) Sensitivity to SN38 and oxaliplatin at clinically relevant concentrations in HROC39 parental cell line and colibactin-tolerant derivative. Results represent mean ± SD (n=2 for SN38, n=3 for oxaliplatin). **: $p<0.05$ (Student's t test). Ns, not statistically significant. (**G**) Sensitivity to SN38 in SW480 parental and isogenic *ATM* KO cell lines. Results represent mean ± SD (n=3). (**H**) Sensitivity to SN38 in KP363T and HROC278MET parental cell lines and corresponding olaparib-resistant derivatives is reported. Results represent mean ± SD (n=3). Related to Figure 6.

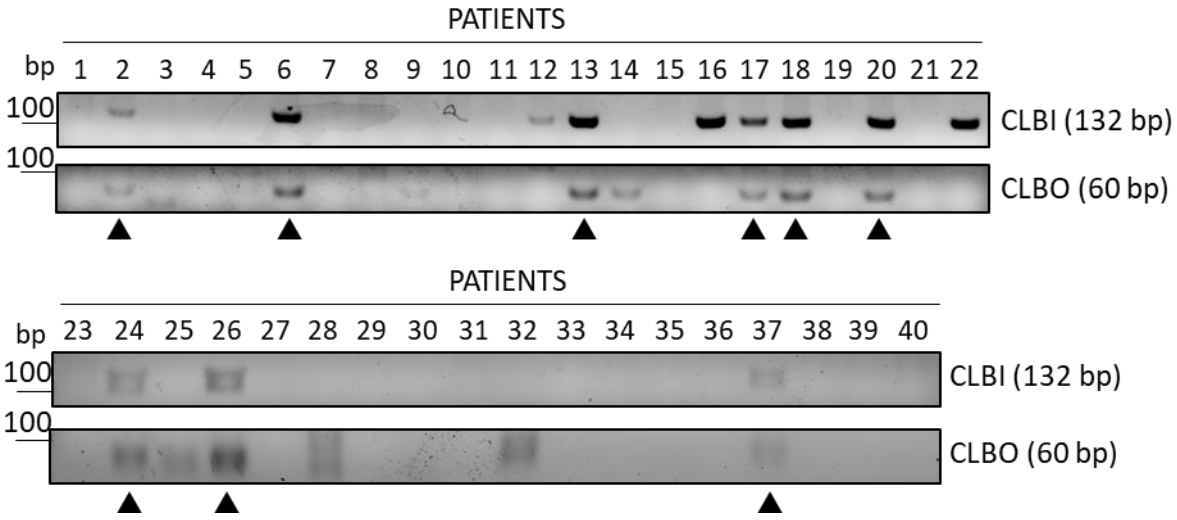

Figure S6. Analysis of *pks* prevalence in clinical samples of metastatic colorectal cancer. PCR detection of two amplicons from the *CLBI* and *CLBO* regions of the *pks* genomic island. Arrowheads mark samples in which both amplicons were detected and which were therefore considered *pks*-positive for the analysis. Related to Figure 7.

Clinicopathological features	***Pks*-positive (N=9, 100)**	***Pks*-negative (N=31, 100)**
Age [median; (range)]	67 (50-81)	61 (39-77)
Gender (N, %)		
Male	7 (78)	20 (64)
Female	2 (22)	11 (36)
Sample analyzed (N, %)		
Surgical resection	9 (100)	29 (93)
Biopsy	0 (0)	2 (7)
Primary tumor sidedness (N, %)		
Rectum	1 (11)	10 (32)
*Left colon **	3 (33)	13 (42)
Right colon ^	5 (56)	8 (36)
Primary tumor histology		
Adenocarcinoma NOS	7 (78)	28 (90)
Mucinous	2 (22)	3 (10)
Grading		
G1-2	3 (33)	18 (58)
G3	2 (22)	10 (32)
Unknown	4 (45)	3 (10)
Stage at diagnosis (N, %)		
Stage I - II	0 (0)	2 (7)
Stage III	3 (33)	7 (23)
Stage IV	6 (67)	22 (70)
RAS mutant (N, %)		
Mutant	3 (33)	9 (29)
Wild-type	6 (67)	17 (55)
Unknown	0 (0)	5 (16)
BRAF mutant (N, %)		
Mutant	2 (22)	1 (4)
Wild-type	7 (78)	25 (80)
Unknown	0 (0)	5 (16)
Mismatch repair (MMR) status (N, %)		
MSI	0 (0)	0 (0)
MSS	3 (33)	11 (36)
Unknown	6 (67)	20 (64)
Best response to oxaliplatin-based regimens (N,%)		
Evaluable	8 (89)	27 (87)
PR	3 (37)	15 (55)
SD	2 (26)	5 (19)
PD	3 (37)	7 (26)
Best response to irinotecan-based regimens (N, %)		
PR	3 (33)	17 (55)
PD	6 (67)	14 (45)
Irinotecan line of treatment (N, %)		
First	1 (11)	4 (12)
Second	8 (89)	25 (81)
Third	0 (0)	2 (7)
Targeted agent of top of irinotecan-based regimen (N, %)		
None	7 (78)	22 (71)
Anti-VEGF	2 (22)	9 (29)

Table S3. Clinicopathological information of pks-positive and -negative mCRC patients. The presence of the *pks* island was determined by endpoint PCR on two distinct amplicons in 40 mCRC patient samples. Clinically relevant information of CRC patients with colibactin-positive and negative tumors is reported. Related to Figure 7.